UNIVERSITAT POLITÈCNICA DE CATALUNYA
BARCELONATECH
Escola Tècnica Superior d'Enginyeria
de Telecomunicació de Barcelona

Complete fabrication station of scalable microfluidic devices for sensing applications

A Master's Thesis

Submitted to the Faculty of the

Escola Tècnica d'Enginyeria de Telecomunicació de Barcelona

Universitat Politècnica de Catalunya

by

Chunyu Yang

In partial fulfilment

of the requirements for the degree of

MASTER IN ENGINEERING PHYSICS

Advisor: Jasmina Casals Terré

Barcelona, October 2022

UNIVERSITAT POLITÈCNICA
DE CATALUNYA
BARCELONATECH

telecos
BCN

Title of the thesis: **Complete fabrication station of scalable microfluidic devices for sensing applications**

Author: **Chunyu Yang**

Advisor: **Jasmina Casals Terré**

Abstract

The research group at the ESEIAAT Microtech Lab in Terrassa is responsible for research in the field of microfluidics. During their research trajectory, some projects have failed to go from the lab to the market due to the fact that there is a lack of well stablished manufacturing processes to scale microfluidic devices. Currently, the lab is working on different devices that need to be industrialized and several companies are interested in their scalable production.

The focus of the work is validate a manufacturing process that can batch produce the microfluidics devices developed in the Lab. To do so, we propose to go from conventional softlithography to a novel methodology that performs the exposure using a maskless writer. In the study its resolution will be compared to previous technologies. At the same time, the replication of the mold is completed by using epoxy material. Finally, the performance of sTPE material as substrate for printed electrodes and sensors will be tested. The electrodes are printed in an elongated manner, trying to optimize the printing effect of the electrodes. Different drying methods were used for the printed electrodes and the performance of the electrodes was compared focusing on the flexibility capacity of the electrodes

The photoresist mold exposed by the maskless writer can also obtain microfluidic channels with good performance after being transferred by PDMS. But the molds exposed at different resolutions have different levels of completeness/sharpness of the edge parts. Relying on the hot embossing process and soft lithography process, the designed pattern is replicated between different materials. There is not much deviation in its size. Electrodes printed with sTPE materials can be used as conductivity sensors, but they cannot withstand bending as well as PET sensors. The electrodes printed while elongatedare more resistant to thebending, but they still lose the function as as conductivity sensor.

Glossary

PGMEA: Propylene Glycol Methyl Ether Acetate

HT: Holding Time

CT: Cooling Time

PDMS: Polydimethylsiloxane

sTPE: Soft Thermoplastic Elastomer

Tg: Glass transition temperature

Table of contents

List of Figures

List of Tables

1. Introduction

In recent years, microfluidic technology has been greatly developed. However, the mass production of microfluidic devices is still a challenge to bring the novel devices from the lab to the market. This is due to the fact that the lab production processes are mainly manual, therefore time-consuming and with low accuracy. Iterative steps for cleaning, patterning, etching, and depositing, are usually required, and all the processes, should be done in a cleanroom environment.

The research group at the ESEIAAT Micro tech Lab in Terrassa is constantly working on the creation of different devices that can be introduced in the market in the near future. This master thesis, as mentioned, focuses development of novel manufacturing processes suitable for the batch production of microfluidic sensing devices.

This type of devices can be divided into two parts:

1. The microfluidics layer, which contains a series of channels and reservoirs. In order to build this part, there is the need to manufacture the negative of it using a mold. The designed pattern is then transferred to the substrate, and of the device is fabricated.
2. The sensing unit. At the reservoir or the sensing area, a sensor is embedded, generally based on conductive material. In this work, silk mask is used to print electrodes on the materials.

The soft lithography technique is used in this thesis as a benchmark technology because it is the standard technique used in microfluidic laboratories However, this fabrication process is not easily industrialized, which makes it only suitable for research. In addition, it usually needs a mask to define the patterns with the required resolution, which has to be obtained from an external supplier. Therefore, the accuracy of the devices depends on an uncontrolled external factor and reduces the efficiency of prototype testing.

As an alternative, maskless lithography is introduced as a novel technique, which will be described in detail below. With this technique, there is no need to use a mask, which simplifies the process. The design can be directly introduced into the computer and expose itusing LCD projection technology, with higher resolution and less irregularities at the edges.

PDMS is widely used for prototyping in microfluidics community. In MicroTechLab, there are prototypes for sweat sensing applications which has already been validated using PDMS and soft lithography techniques to fabricate them. However, since this technology is not scalable, its applicability as a product is limited.

Finding suitable alternative materials and processes is an important area of development in the area of micro and nanomanufacturing community. Emmanuel Roy et al proposed in

2017 a novel soft thermoplastic elastomer (sTPE) to be a good candidate to batch produce microfluidic parts [2]. This type of polymer compensates for the shortcomings of castable elastomers and is ideal for making microfluidic devices. At a certain temperature, it takes on a viscous state and solidifies when the temperature drops, and it can be stamped with good reproducibility of microfeatures. It also has excellent elastic and optical properties.

The focus of this study is therefore to validate scalable technologies at different stages of laboratory-scale device fabrication, enabling a smoother transition from prototype to production.

1.1. Objectives of project

The objective is to propose and validate scalable micromanufacturing techniques that with resolutions that allow a proper performance of the device can then achieve a smoother transition from prototype to production. The idea is to use state-of-art equipment to accomplish this goal and propose a complete fabrication process for all the parts involved in the manufacturing of a wearable sweat analysis platform: from the microfluidic mold for the sweat gathering system to the printing of the electrodes for the sensor unit. All using scalable techniques but now validated at lab/prototype production. Therefore, at firstthe costs will not be strictly considered and only the replicability capacity, that should be higher than 100 units per day.

Scheme of the project:

The project involves the manufacturing of two parts:

1.- A microfluidic channel device that uses conventional soft lithography techniques to fabricate photoresist molds [1]. This initial mold made out of photoresist (SU8) will later be used to fabricate a polydimethylsiloxane (PDMS) molds. PDMS is selected as a material for manufacturing EPOXY molds, since it shows go reproducibility of micro features and it does not stick to EPOXY enabling the demolding process. The final epoxy mold is then produced by casting. Epoxy molds can be used for mass production techniques, such as hot embossing, to transfer patterns onto sTPE materials.

2.- The sensing unit. This part requires the definition of electrodes on the surface of the sensor area. The screen printing technique is chosen as a manufacturing technique since it is a highthrough put technique that can batch produce a significant number of electrodes in each step. The sensor will be printed on sTPE material and its electrochemical performance will be tested.

Objectives:

- Define a photoresist mold fabrication process using a maskless writer to eliminate the need of masks, speeding up the iteration process and reducing costs. Metrics: Resolution (tolerance) and good replication. The benchmark of the process will be done comparing with conventional soft lithography process that requires the use of masks.
- Define a casting process of the microfluidic part that uses more durable epoxy molds. Compare the dimensions achieved with conventional photoresist molds made out of photosensitive resin SU8. To ensure that there is not a loss in resolution, the dimensions will be compared across the different stages of thefabrication process.
- Define a hot embossing process to replicate the pattern from the epoxy molds on the sTPE sheets. The set-up requirements of the process and the durability of the epoxy molds will be defined. The pre and post dimensions of epoxy mold will be measured to know if there are changes during the thermoforming process.
- Test the screen-printing on sTPE. Validate that the combination of the chosen ink and the sTPE material can have good adhesion and acceptable electrical performance (resistivity and connectivity of electrodes), electrical properties after bending.
- Design and validate a conductivity sensor able to work on the sweat range of values. Determine the calibration plot of the designed sensor using different NaCl concentrations present in sweat.

2. State of the art of the technology used or applied in this thesis

This chapter reviewed initially the most frequently used materials to manufacture microfluidics channels and electrodes. As well as, the physical and chemical properties that are required to these materials. Then the methods used to create this type of part are introduced, taking special care to the mold creation process, because most of the manufacturing processes involve or require a mold, for instance casting or hot embossing. The methods reviewed are divided into low-volume and high-volume manufacturing techniques. The lower volume processes follow a sequential development, and we focused on the soft lithography process since it is wide spread. Between the high-volume processes, hot embossing has been selected due to their current important role for the commercial production of microfluidic devices. On the other hand, the fabrication of microstructures using machining is not considered, since this process is extremely time-consuming and high cost due to the cost of the equipment and the tools required. Therefore, the manufacturing costs can be greatly reduced if replication methods can be used to straighten micro- or nano-processes. In this case, the micro- or nanostructures are fabricated only once for the masters or moulds of the process, and products can be duplicated from the masters. The masters have the inverted or the negative features of the device structure.

2.1. Material

In soft lithography, photoresist was used to transfer microstructures onto PDMS substrates. The solubility of photoresist will change after exposure to ultraviolet light of a certain wavelength [3]. There are two types of photoresists, negative and positive[4]. The comparison between the negative and positive photolithography preparation process is shown in the figure 2.

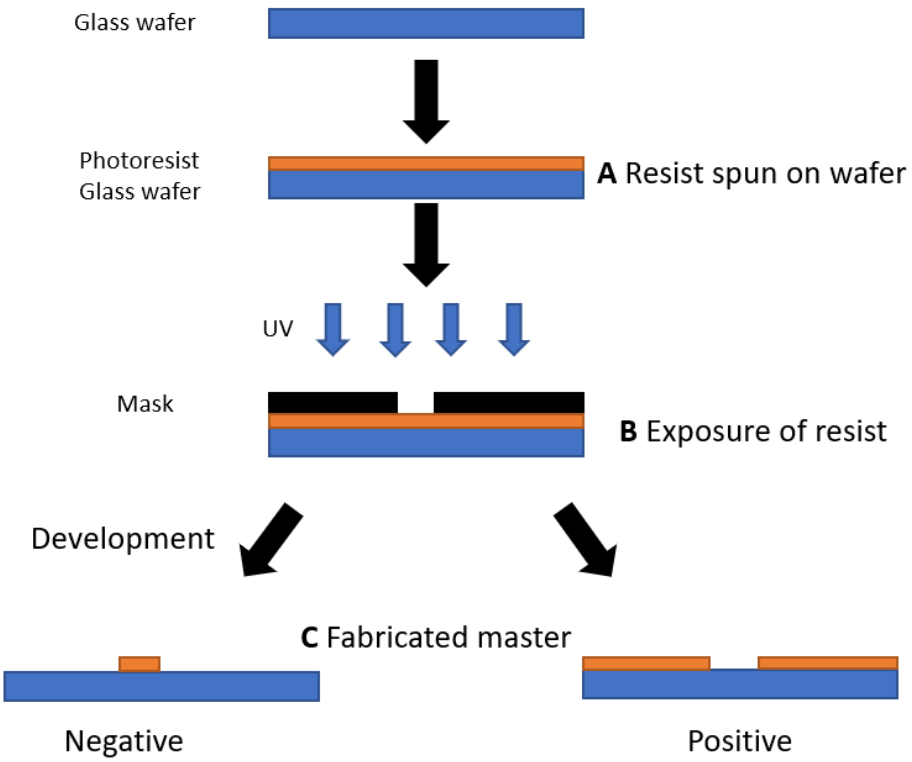

Figure 1 The principle of mask lithography, negative photoresist remains on the substrate after exposure, while positive photoresist dissolves in the developer.

SU-8 is a negative photoresist from microchemicals most commonly used in the field of microfluidics to create the mold of the microfluidic device[5]. Exposure to UV light with 365 nm hardens the material, while the unexposed areas remain soluble and can be washed away during development. For the photoresist mold fabricated using the mask method, SU-8 photoresist was selected for this project.

Polymers are classified according to the chemical properties of the monomers, but the physical classification is divided into three categories, thermosets, thermoplastics, and elastomers[6]. Silicone materials are common elastomers, one of the most common elastomer in the microfluidic field is poly dimethylsiloxane (PDMS). It has been widely used to fabricate microfluidic devices since it can easly replicate patterns from molds using casting methods [7]. Elastomers change shape under the action of an external force and return to their original shape after the force is removed.

Thermoplastic materials soften when the material is heated above the glass transition temperature, which makes them suitable for molding by lodging or heat embossing[8].

sTPE is a material that shares the advantages of thermoplastic materials and elastomers. Therefore, the final product can be easily made using the simplest plastic processing machinery and it also has a low Young Modulus and therefore it is flexible.

Epoxy resins are made using a two-step process, first making a diepoxide—usually from bisphenol A and epichlorohydrin—and then crosslinking the epoxy groups[9]. Compounds added to epoxy groups include amines, amino acids, and thiols, all of which can initiate curing of epoxy monomers. Compared with PDMS, epoxy resin materials have higher hardness.

As a block copolymer material, sTPE material is composed of styrenic (PS) hard blocks and ethylene-butylene (EB) soft blocks. The rigid PS domains act as connection points to stabilize the polymer matrix. While the main EB surrounding matrix provides elastomeric properties. The glass transition temperature of the EB matrix is negative, which corresponds to the constantly moving polymer chains and gives the material soft elastomeric properties. Whereas the glass transition temperature of PS is around 100°C, corresponding to the styrene blocks used as anchors and increasing the stiffness of the material for thermoforming.[10]

Table 1 Comparison of Young's modulus and hardness of three materials[10-14].

	Hardness (Shore A)	Young's modulus (MPa)
PDMS	41.7	2.46
Epoxy	80	3350
sTPE	35	1.15

2.2. Manufacturing techniques for microfluidics

Soft lithography is the process that uses light to define nano/microfeatures on photosensitive materials to create either molds or microfluidic parts, see Figure 2. Generally, photolithographic techniques are used to produce photoresist molds from masks. Later, in these molds a liquid polymer is casted and cured to replicate the mold pattern. It is possible to obtain micron-sized or even nano-sized features on the molds and later on the parts, but the demolding process is prone to deform or damage the channels in the mold. Therefore, the life of the molds is limited to 10-20 demolding processes, which difficults the industrializion and the scalability of the process[15].

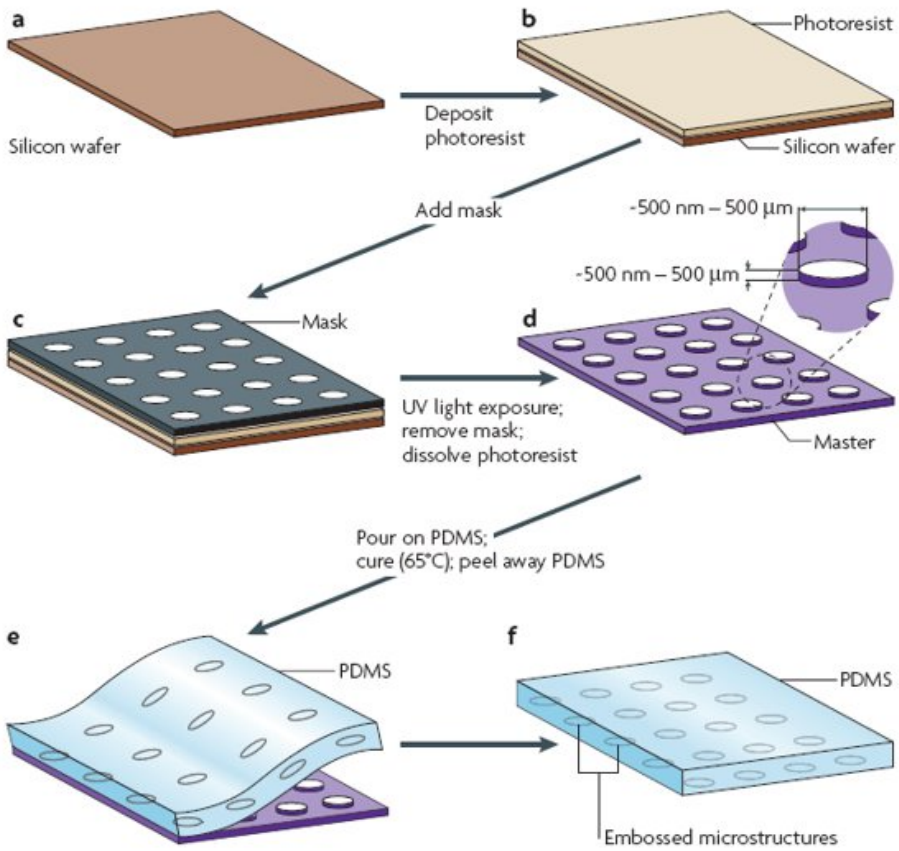

Figure 2 Soft Lithography Manufacturing Technology Process. a to d) Fabrication of an photoresist master mold; e to f) casting of PDMS on the mold [1].

Figure 2 (c) introduces a mask, which can be either created by laser patterning of chromium on glass or by high-resolution printing on a plastic sheet. When a change in the design is required a new mask is needed. Therefore, a delay on the manufacturing process is expected since there is this additional step to manufacture the mask.

Now a days, machines such as microPolos Printer [16], a maskless technique that defines an area or pattern of exposure at a certain wave length and does not requires any physical mask. It works as a projector that reflect the pattern loaded on the substrate with a photoresist[17].

For maskless techniques, no mask is required for exposure, instead a maskless writer is used. In our work, a microPolos was used. The mask less method uses a POLOS uPrinter based on a microLCD projection technology compatible with a wide range of resists. The resolution of the microLCD (according to the specifications 2 um) is now sufficient to define features which are in the range of 10-500 um[18]. Figure 4 describe the steps followed to obtain the mold. First, figure 4 (a) the selected photoresist that should be compatible with the wavelength of the LCD (465nm), is spun on the substrate using a spinning machine. Then the maskless equipment exposes the resin according to the pattern that has previously been designed in AUTO CAD and which is directly projected on the

substrate through the exposure system. The LCD modifies the resist that is later removed using developer under the fume hood.

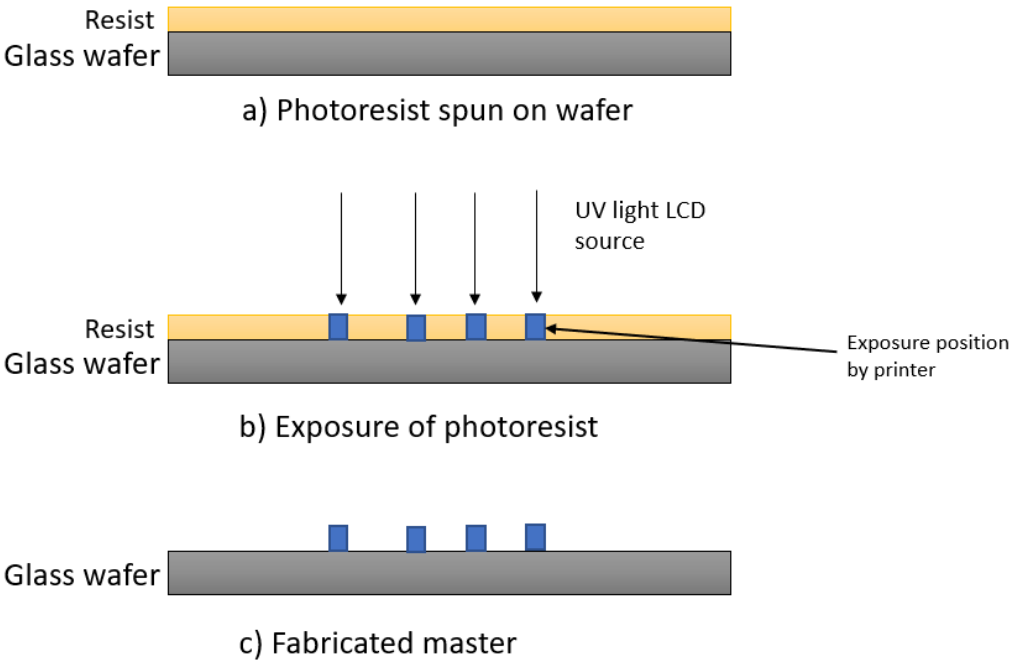

Figure 3 The principle of maskless lithography

Hot embossing process. Figure 4 shows the schematics of the hot embossing process, which is a technology that replicates the mold features on thermoplastic polymers. The process heats the thermoplastic up to its glass transition temperature and at this viscous state deforms the material. The mold and the selected polymer are located into a hot press, pressure is applied during a certain time to the material which is hold at a certain temperature, and then it is cooled and demolded.

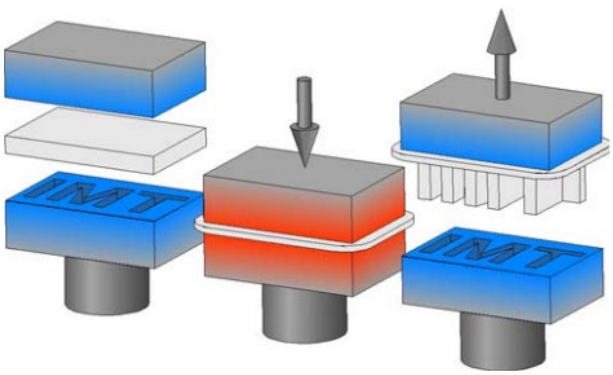

Figure 4 Schematic diagram of hot embossing production technology[19].

When the temperature exceeds the phase transition temperature, the polymer becomes similar to a viscoelastic fluid. The polymer in this state can fill its cavity to fit the pattern of the mold. When the temperature is lowered, the polymer will retain its filled shape and harden, shown in figure 5. Table 2 summarizes the different characteristics that should be considered when choosing a manufacturing technology for microfluidic part manufacturing.

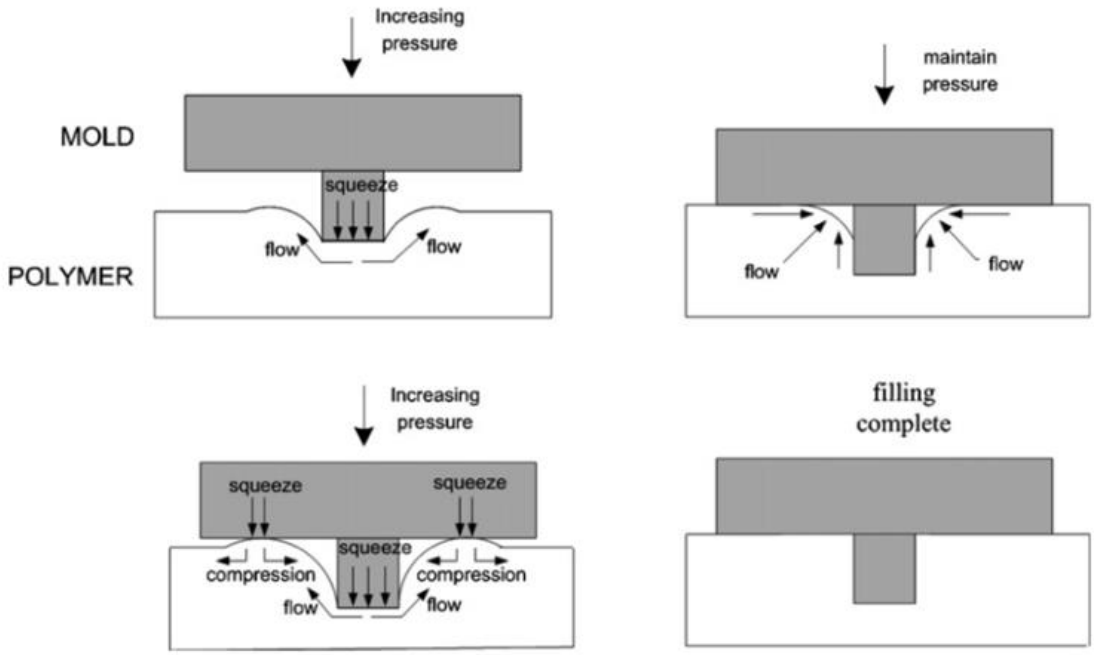

Figure 5 Behavior of the polymer in the HE process. a) Application of pressure on the substrate. b) Circulation of the polymer in a viscous state. c) Maintenance of pressure due to the filling of the cavities. d) Filling and completed replication[20].

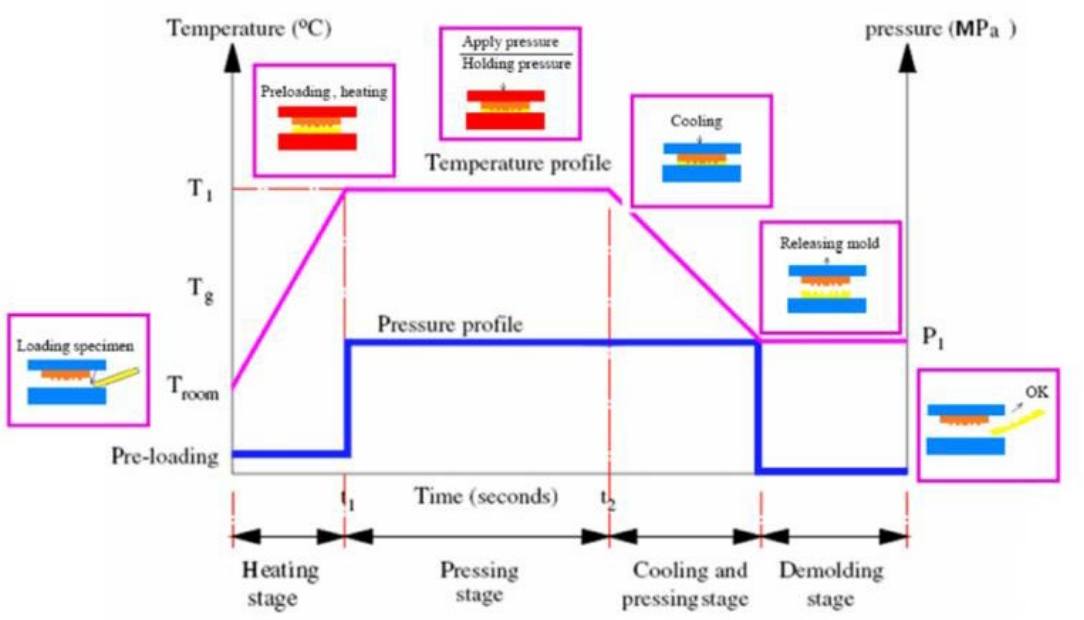

Figure 6 Graph of pressure/temperature vs time showing the different stages of the HE process[21].

Technology	Resolution	Compatible Materials	Time	Cost
Soft lithography	High	Elastomer	Long	High
Hot embossing	High	Thermoplastic	Short	Low

Table 2 Different manufacturing technologies for microfluidic parts[22].

2.3. Electrode printing

CVD deposition, like example Ti electrodes coated with SnO2 film. Thin films were grown on glass and titanium plates in a horizontal hot-wall MOCVD reactor at low pressure using SnEt and O2 as reagents. The gas is adsorbed on the substrate as it passes through the reactor. Reacts with reactants on the substrate. Then the organic product is

released from the surface of the substrate, while SnO2 diffuses on the surface of the substrate.

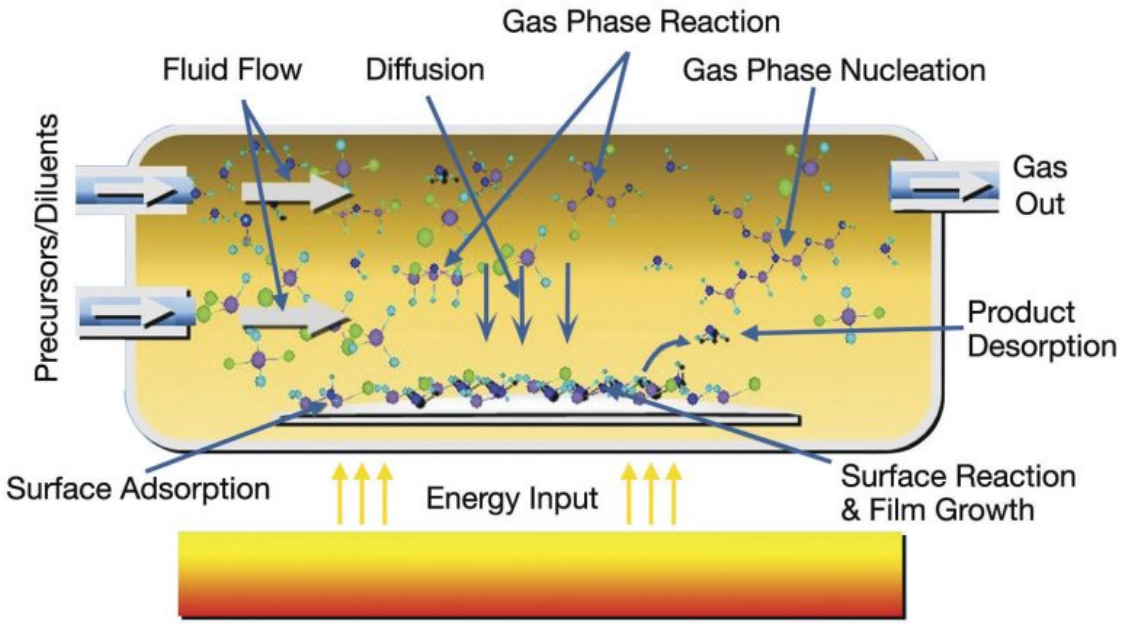

Figure 7 Aspects of a CVD process.[23].

Liquid metal electrode, commonly used in the manufacture of stretchable electrode devices. A femtosecond laser is used to drill holes in the polymer, allowing air to escape during liquid metal filling. The process flow is shown in the figure 8. A microelectrode includes two layers. First, a cured PDMS layer is fabricated on the substrate. A Polycarbonate (PC) Membrane was overlaid on it, and then the PC and PDMS layers were peeled off the substrate together. PDMS does not break due to the support provided by the PC film. Insert the inlet of the liquid metal microelectrode, made of a hole punch of approximately 1.2mm diameter.

So far, the preparation of the microelectrode channel layer is completed. A sealing layer for sealing below the channel layer is then fabricated from PDMS material.

After preparing the two different layers of the microelectrodes, they are bonded by oxygen plasma treatment. Connect the channel and the sealing layer. After laser ablation, the microelectrode structure is fabricated. The channels were subsequently filled with liquid metal and the PC film was peeled off.

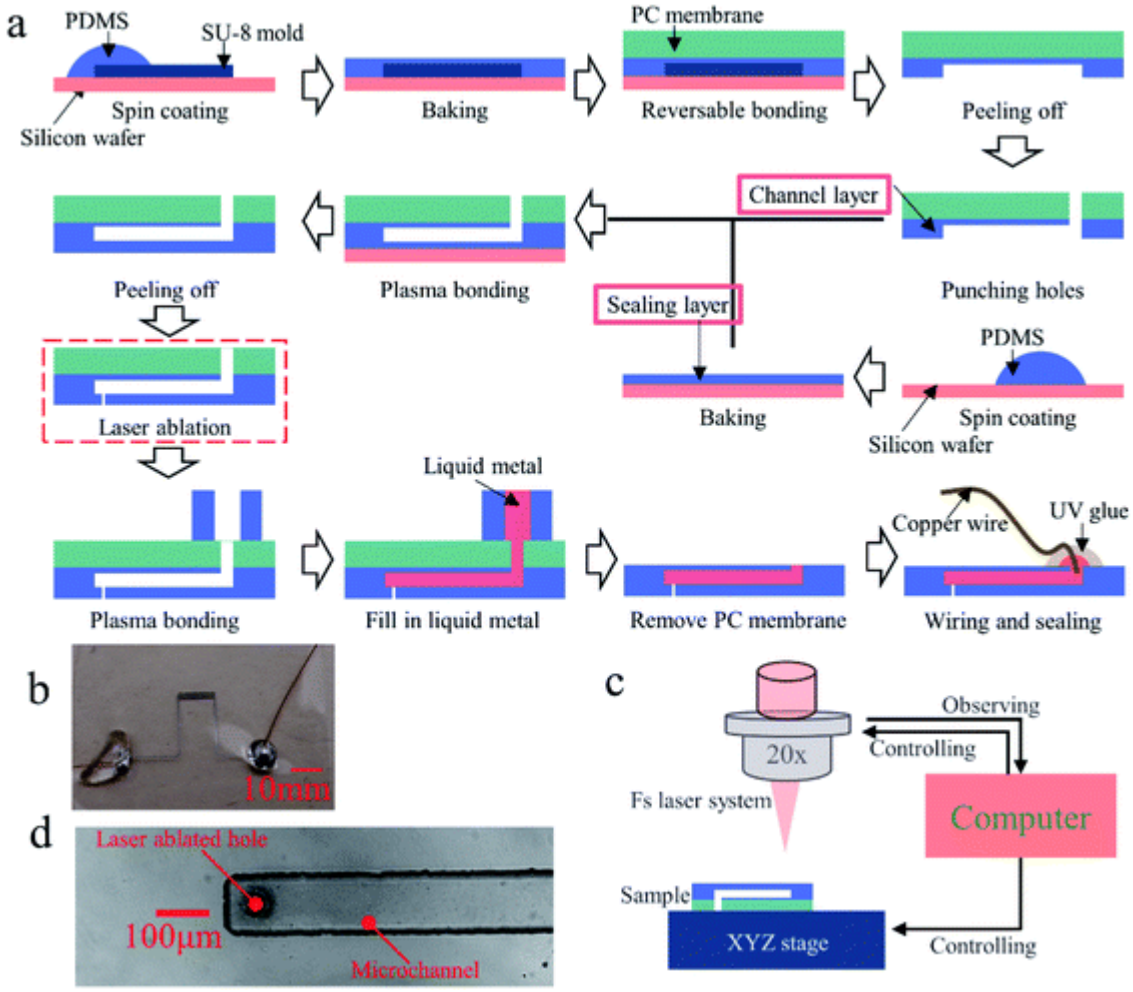

Figure 8 Fabrication process and the result of the microelectrode. (a) Schematic of the microelectrode fabrication process; (b) a photo of fabricated microelectrode; (c) schematic of laser drilling process during fabrication; (d) laser-drilled hole inside the m microchannel[24].

Screen printing, as a common technique for electrode fabrication, is characterized by low cost and simple operation. The basic principle of screen printing is to use the basic principle that the mesh of the graphic part of the screen printing plate is transparent to the ink, and the mesh of the non-graphic part is not permeable to the ink. When printing, pour ink on one end of the screen printing plate, apply a certain pressure on the ink part of the screen printing plate with a scraper, and move to the other end of the screen printing plate at the same time. The ink is squeezed onto the substrate by the scraper from the mesh of the graphic part during the movement.

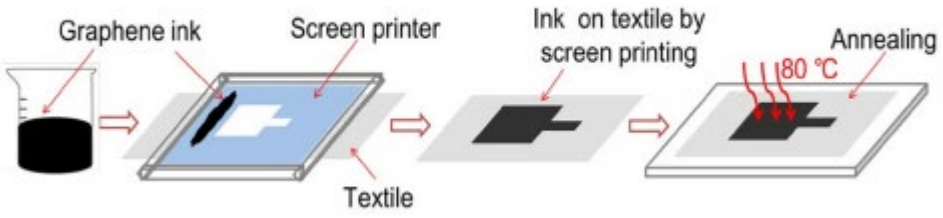

Figure 9 Screen printed electrodes on textile for wearable electrocardiogram monitoring[25].

2.4. Conductivity sensors

For the fabricated electrodes, standard conductivity solutions were used to measure their electrochemical performance. The conductivity of the electrolyte solution is usually measured using a conductivity cell. If the area of the electrode is A and the distance between two clicks is l, the conductivity of the solution is

$$L = \frac{K * A}{l}$$

K is the specific conductance, which is the conductance of the solution when l=1m and A=1, and the unit is S/m[26].

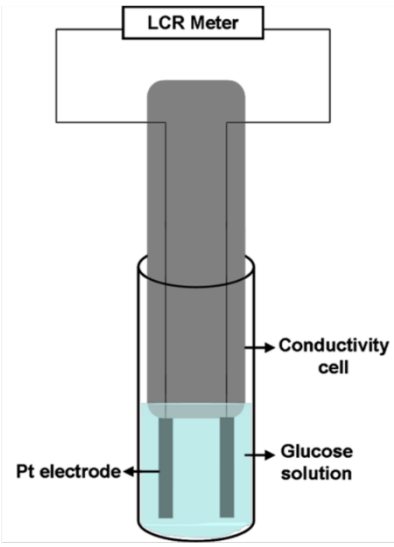

Figure 10 Schematic diagram of the conductivity cell inside the test[26].

The cell constant (Kcell) gives the relationship between the detected conductivity (G) and the specific conductivity (Ksol):

$$G = \frac{K_{sol}}{K_{cell}} = \frac{\sum_i \lambda_i C_i}{K_{cell}}$$

Ksol is the product of the concentrations, Ci, and ion conductivities, λi, of all the individual types ofions in the electrolyte. The cell constant depends on the geometry of the sensor and generally increases with smaller sensors. For on-chip measurements, it is technically easier to use planar electrodes because these electrodes are better integrated into the microsystem. To reduce Kcell, interdigitated electrodes are usually used.

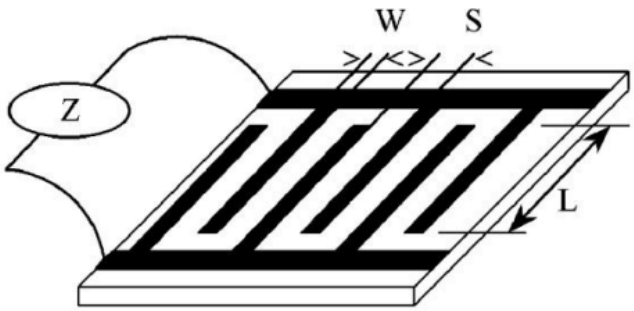

Figure 11 Schematic diagram of the layout of the interdigital electrode pair with an area of 0.1cm^2.[27]

The electrical equivalent model is shown in Figure 12:

$$Z(j\omega) = 2R_{lead} + \frac{x}{j\omega C_{Cell} x + 1}$$

$$x = R_{elec} + \frac{2}{j\omega C_{DI}}$$

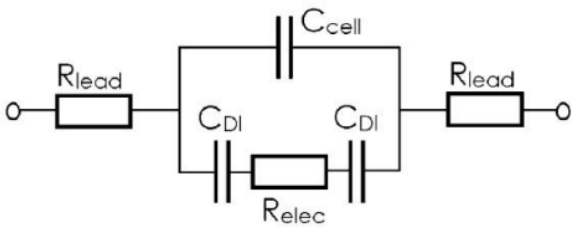

Figure 12 Equivalent Circuit and Impedance Expression of Electrolyte Conductivity Sensor[27].

Figure 12 shows the impedance equation for the equivalent circuit. At lower frequencies, the impedance will be dominated by the concentration-dependent double layer capacitance C_{D1} until the impedance of this capacitor becomes lower than that of the electrolyte and the sensor impedance becomes frequency independent. The frequency f_{lo} at which this occurs is given in the following equation:

$$f_{lo} \approx \frac{1}{2\pi\left(R_{lead}C_{DI} + 2R_{lead}C_{Cell} + \frac{1}{2}R_{elec}C_{DI}\right)} \approx \frac{1}{\pi R_{elec}C_{DI}}$$

At a certain frequency, the impedance of Ccell becomes lower than Relec and the impedance decreases again with increasing frequency. The frequency with which this happens is given in the following equation:

$$f_{hi} \approx \frac{1}{2\pi R_{elec}\frac{C_{DI}C_{Cell}}{C_{DI}+2C_{Cell}}} \approx \frac{1}{2\pi R_{elec}C_{Cell}}$$

For the sweat sensor to be designed in this experiment, its Kcell is higher. Therefore, the size of the sensor needs to be corrected. The following figure13 is a sensor suitable for sweat collection.

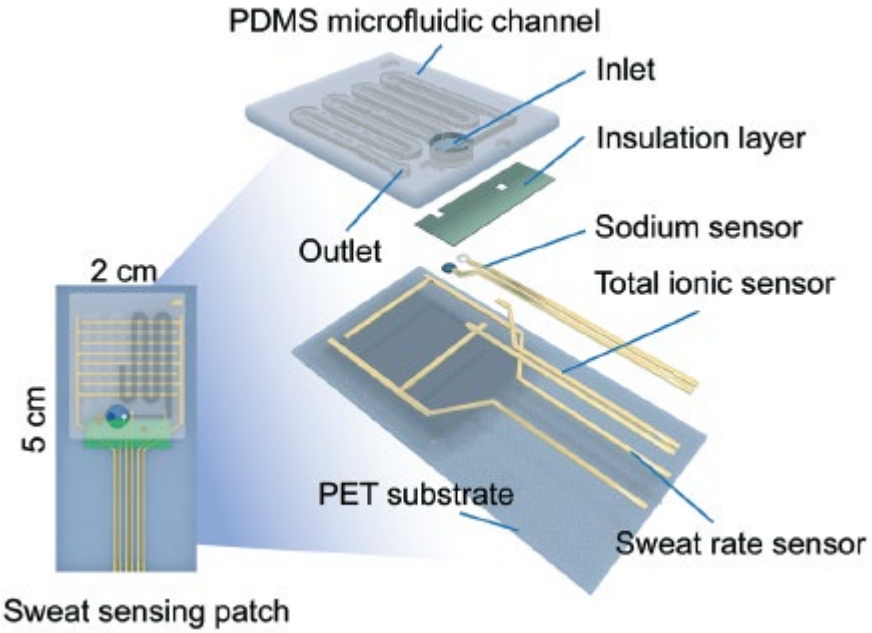

Figure 13Schematic of multi-modal sweat sensing patch with sensors for sweat rate, total ionic charge concentration, and Na+ ion concentration located within a PDMS microfluidic for sweat capture and flow.[28]

In order to make the measurement results more accurate, two factors, sensitivity and detection limit, need to be considered. The sensitivity is difficult to keep constant over a wide range of concentrations. Therefore, sensitivity is only meaningful when a concentration or concentration range is specified. According to the relationship between sensitivity and detection limit, the higher the sensitivity, the lower the detection limit. Therefore, the use of miniaturized equipment in the laboratory can reduce the detection limit and make the measurement result more accurate.[29]

3. Methodology

This section will detail the methodologies and laboratory procedures used during this thesis. First, mold fabrication will be covered.

A positive mold is first prepared on a glass plate. Afterwards, a PDMS reverse pattern is made. The pattern is then transferred to the epoxy mold through the pouring process. Finally, the sTPE part is fabricated by hot embossing technique.

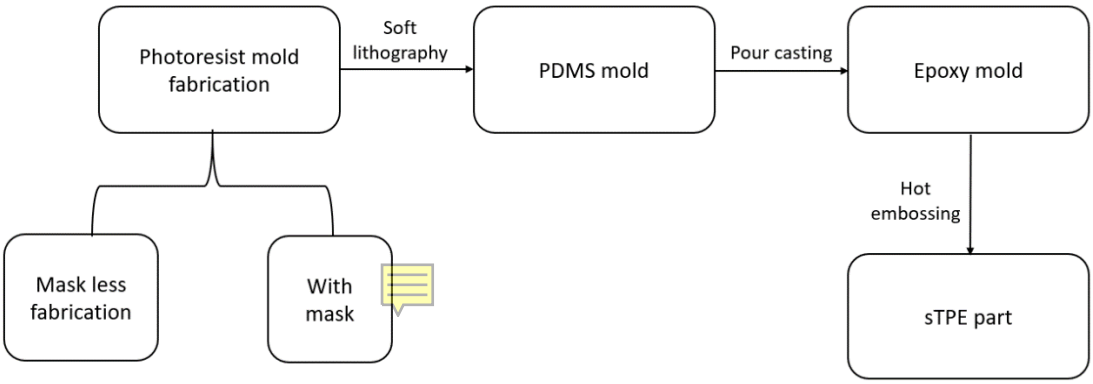

Figure 14 Scheme of the microfluidic layer workflow.

Afterwards, the procedure for electrode deposition using screen-printing will be detailed as well as the electrochemical characterization of the conductivity sensor.

3.1. Photoresist mold fabrication

Photoresist mold fabrication with mask

For conventional photoresist fabrication, a mask is used. The photoresist used is SU-8 which is a negative. The production steps are as follows:

1. Use a 3:1 volume ratio of concentrated sulfuric acid (95%-98%) and concentrated hydrogen peroxide solution (30%) in a piranha solution to clean organic residues from glass substrates.

2. The substrate was washed with distilled water and air-dried. Treatment with oxygen plasma (Tucano Plasma Reactor from Gambetti) in 110w, 120s. The photoresist is evenly coated on the glass substrate by a spinner (from Brewer Science). The thickness of the photoresist depends on the rotational speed. The higher the rotational speed, the thinner the photoresist. Complete the spin coating process according to the established protocol.

3. The photoresist is then preheated and covered with a mask. Exposure to UV projectors and halogen lampheads (from BCB) for 8 seconds and post bake.

4. Develop the mold using Propylene glycol monomethyl ether acetate and wash with acetone several times. Refer to Appendix A1 for detailed steps.

Maskless photoresist mold fabrication

The UV wavelength provided by the Polos writer in the lab is 465nm, which does not match the SU-8. So, choose AZ125nxt-10A photoresist that matches the wavelength. The pattern exposed by the device must be in bitmap format. Therefore, the pattern designed by AUTOCAD can be converted into the bitmap required by the device through the SFTprint software. High resolution mode is recommended when the exposure pattern is smaller than one-fifth of the projected size. In the case of high resolution, the pattern is divided into several small sub-images. There will be gaps and tilt between each sub-image. To eliminate these gaps and tilt, a calibration pattern is used to calibrate the pixel size and angle.

Due to some unavoidable errors, after the pixel size is calibrated, the pattern may still have gaps. Subgraphs can be stitched together by using the field connection function. Calculate the number of pixels needed by using a profilometer or microscope to determine the size of the gap. Add the appropriate pixel value to the field connection option.

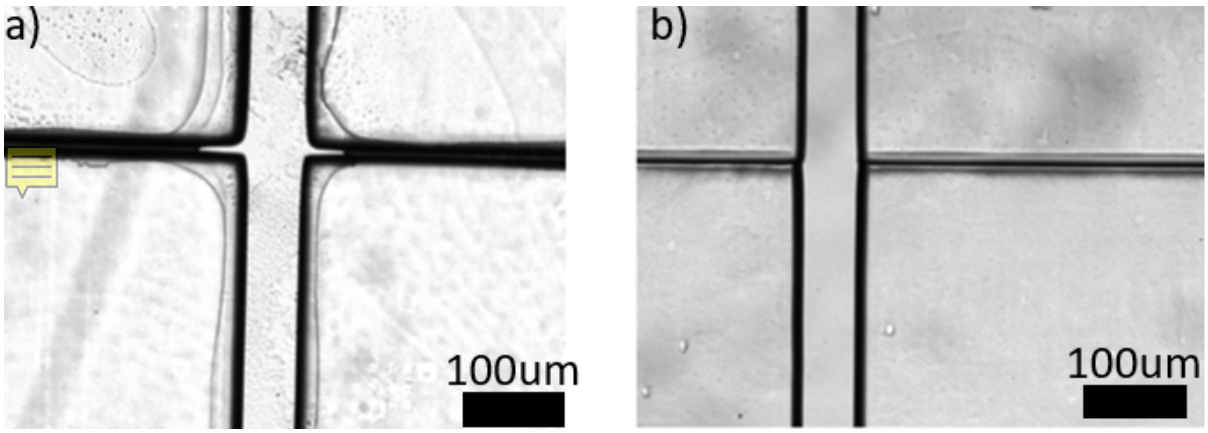

Figure 15 Exposure result after tilt calibration and pixel size calibration. a) The field connection option is not used, b) The pattern after splicing with field connection, the gaps at the splicing edges are removed, and the subimage edges are smoother.

In order to obtain the accurate pixel size as much as possible, it is necessary to obtain the optimal exposure conditions. The exact exposure duration can be obtained through the dose test mode. For a more detailed steps of the calibrate pixel size and dose test settings, see appendix A2.

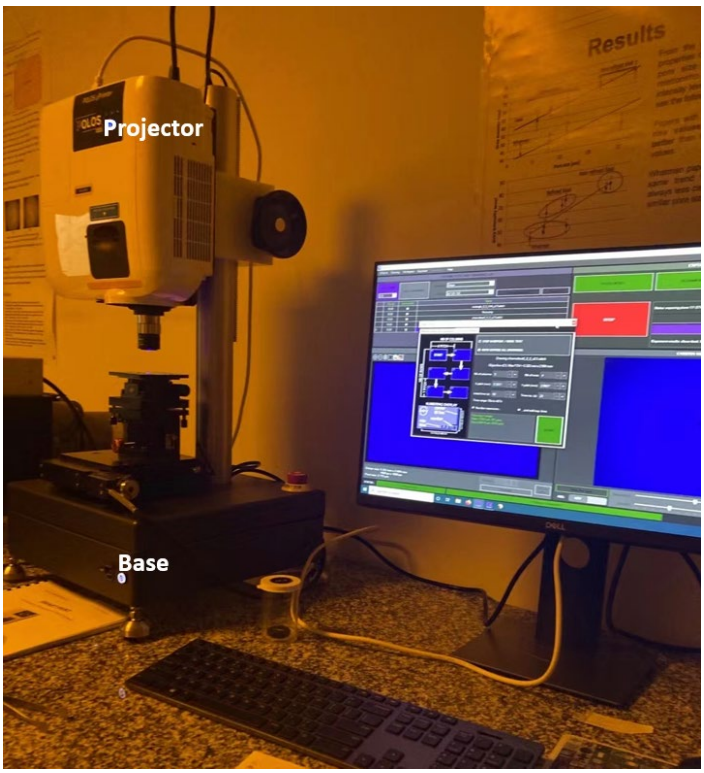

Figure 16 The maskless writer, consists of three parts: projector, base and monitor

After completing the above preparations, the photoresist mold can be fabricated according to the following steps:

1. Glass substrates were washed with piranha solution and rinsed with distilled water, dried and preheated.

2. According to the established protocol, the photoresist was evenly spread on the glass substrate by a spin coater. Place on a hot plate for soft bake 40 mins with 120°C.

3. Transfer the designed pattern to the computer. In focus mode, focus calibration for UV projection is performed. After the calibration is complete, select the starting position of the exposure and set the exposure duration.

4. After exposure is complete, a complete master is formed using AZ300MIF developer.

For a more detailed protocol of the development process, see appendix A3.

The thickness of the molds manufactured was measured using a Filmetrics profilometer (Profilm3D), see Figure 17(a). The in plane pattern dimensions were measured using an optical microscope and ImageJ software, see Figure 17(b).

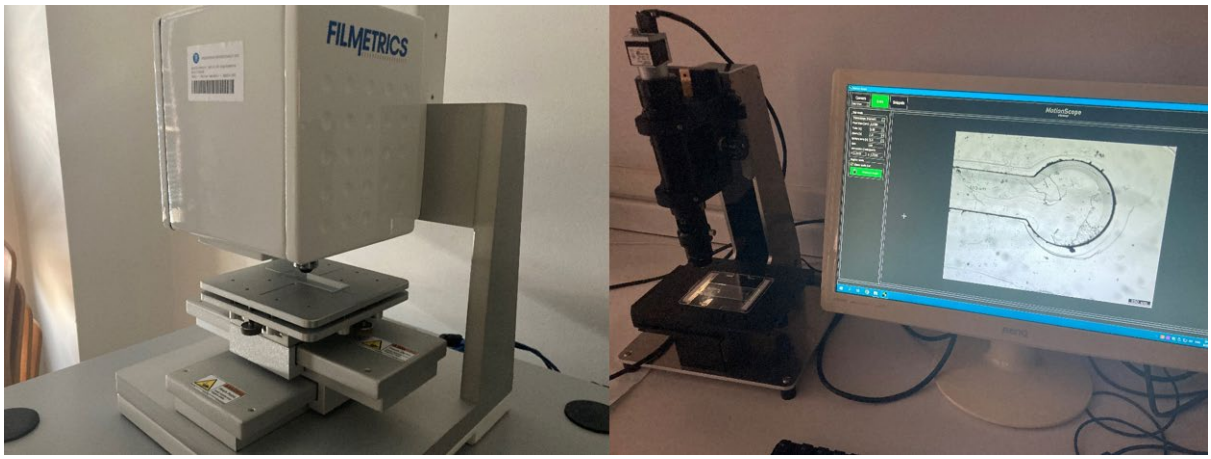

(a) (b)

Figure 17 (a) Filmetrics Profilometer; (b) Microscope and measurement images

Since photoresist molds fabricated with a mask and photoresist molds fabricated with a maskless technique use different patterns. The accuracy of the two fabrication processes is compared by comparing the relative error of the width of the channel in the photoresist pattern compared to the theoretical width of the design. 8 channels of different widths in Figure 18a were selected for measurement. For the pattern of Figure 18b, in addition to selecting channels of different widths, cylinders of different diameters can also be measured.

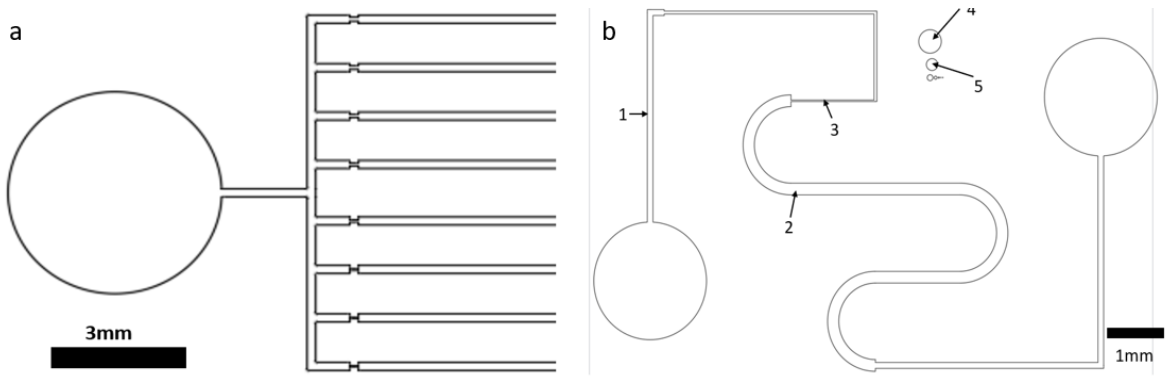

Figure 18 Pattern for measurement, a) with mask; b) maskless

3.2. Transfer to epoxy molds

For the production of the PDMS reverse mold from the photoresist mold, PDMS base and hardener were mixed in a weight ratio of 10:1. The mixture was cleared out of air using vacuum for at least 1 hour. A casting tool was made of multiple glass slides and the photoresist mold was placed at the bottom (Figure 18A). Before that, a vapour deposition of silane was performed on the photoresist mold to avoid adhesion to PDMS.[30] Once the mixture was clear, it was poured into the casting setup and it was thermally cured at 90°C for 2 hours in a hotplate (Thermolyne Model S72835). After cooling, it can be unmolded easily thanks to the prior silanization of the photoresist mold. See Appendix B for detailed steps.

To transfer the PDMS counter-mold to epoxy mold, a frame for casting was required. Usually a steel-based frame was used to hold the PDMS mold and the injected epoxy mix. But the cost is high, so cheap alternatives are sought at the laboratory. As a first option, aluminium foil was used instead of steel to make a simple frame because it was a methodology already used for casting at the laboratory. The procedure started by placing the PDMS counter at the bottom of the manual-made frame.

The second option is to glue the PDMS reverse mold to an extension part to create a frame made of PDMS material. Regarding the bonding method of the two PDMSs, two methods are provided.

There are two methods of bonding PDMS molds:

1. Oxygen plasma. Oxygen plasma bonding was a common bonding method based on PDMS material microfluidic molds. Oxygen plasma treatment activated the surface of the PDMS and increase the interaction with another PDMS mold. The surfaces of two PDMS molds were treated with oxygen plasma and heated at 95 °C for 2 hours. Bonding was completed.

2. PDMS bonding. PDMS bonding was done by spin-coating a layer of PDMS mixture between the blank mold and the patterned mold, and then heating at 90°C for 30 mins to complete the bonding. The advantages were simple operation and short bonding time.

First, the volume of the epoxy was calculated based on the hollow part of the PDMS mold frame. The resin and hardener were mixed in a volume ratio of 10:6.67. The preparation process was recommended to be done in a fume hood.

The prepared epoxy mixture was poured into the both PDMS mold frame, and baked in an oven for 20 hours at 180°C. See Appendix C for detailed steps.

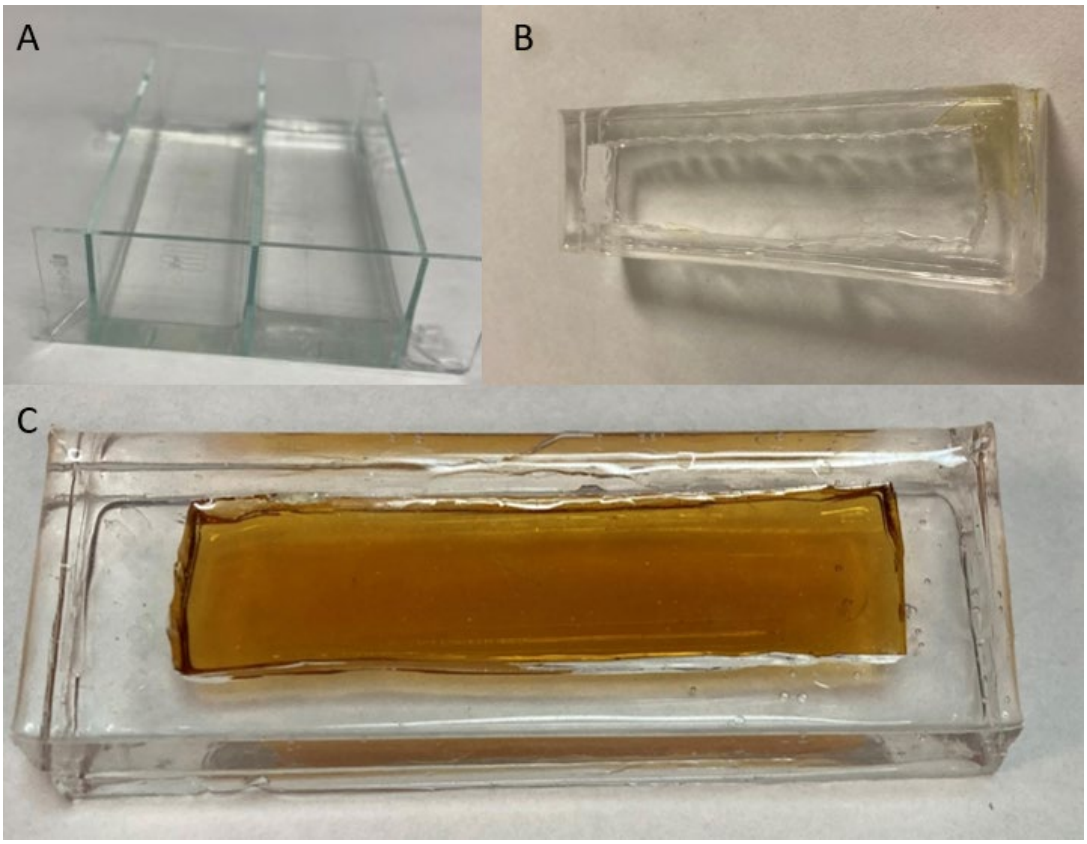

Figure 19 A) PDMS Component Manufacturing. B) Complete PDMS Framework. C) Epoxy mold and PDMS frame not yet demolded

3.3. Hot embossing in sTPE (Flexdym) using epoxy molds

The hot embossing process was divided into 4 different stages: heating, pressurizing, cooling and demolding.

The preheating system heated the upper and lower heat presses to the desired temperature. Then, the Flexdym sheet was placed and the epoxy molds as well, in the center of the heat press. The upper plate is moved down until a pressure of 0.5 MPa is applied (The joystick is at a 40-degree angle to the horizontal, see Figure 20 (b)).

(a) **(b)**

Figure 20 (a) Hot embossing press (b) Hydraulic rod

3.4. Screen-printing of electrodes on sTPE

The electrodes were printed using a silk mask to define the pattern on the substrate (Figure 21 a). LOCTITE Carbon ink was used to print the electrodes. First, the PET and board were washed with distilled water, then the silk mask cleaned with acetone. The carbon ink was applied on top of the pattern and a spatula was used to spread the ink evenly on the pattern and the process was repeated. Finally, the substrate was placed in oven at 90°C for 15 minutes.

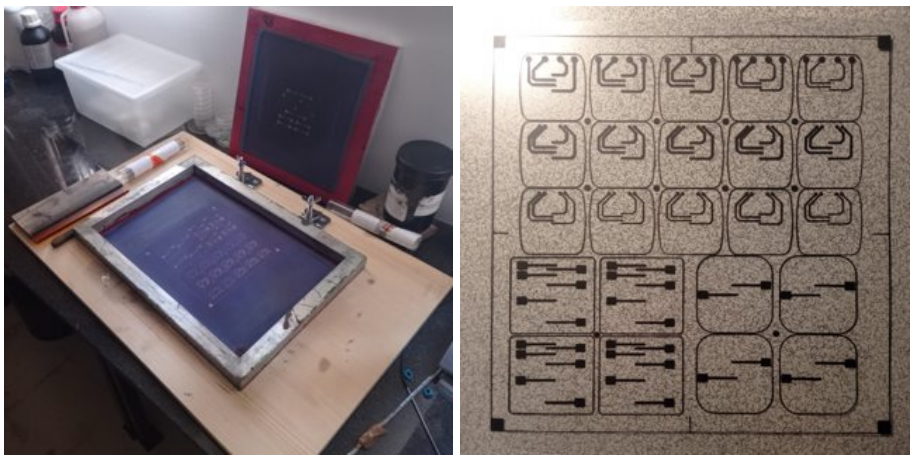

Figure 21 (a) Screen printing equipment used comprising the screen printing mask (b) PET substrate after screen-printing.

For sTPE printing, first we are going to characterize the substrate properties that could affect ink printing compared to PET. The main properties that we believe can have an effect on the ink printing are the Young modulus, surface roughness, contact angle and glass transition temperature. The Young modulus provides information about the degree of elasticity of the substrate which would be important for electrode stability when bending. Surface roughness and contact angle define its interaction with the ink. Lastly, the thermal curing (90ºC) may make the polymer surface viscous (by surpassing the glass transition temperature of the polymer) which could produce unwanted interactions with the uncured ink, decreasing electrode performance. Table 3 is a comparison between these two materials for the mentioned parameters found in literature. Roughness of the substrates were measured experimentally using the profilometer across different pristine areas and the Sa (Area Roughness Parameters) was calculated using the software.

Table 3. Properties of the PET compared to sTPE.

	PET	**sTPE** [2]
Young Modulus	2.76-4.14 GPa [31]	~1 MPa
Roughness (Experimental)	0.322um	0.481um
Contact Angle (º)	~80º [32]	~105º
Tg (Glass transisiton temperature)	70°C [33]	As a coblock polymer: negative for EB, 100°C for PS

Therefore, when printing on sTPE, a few modifications were added to the standard procedures described above. Initially, the substrate was treated with oxygen plasma in 70w and 40s (Tucano Plasma Reactor from Gambetti) to activate the surface of the polymer and increase the interaction with ink. Besides that, ink curing was performed at room temperature to avoid any unwanted effects from the increased viscosity of the sTPE surface (procedure sTPE 2).

Advised from the commercial supplier of the sTPE material, the substrate was stretched during printing, and let it relax back to the original size during the curing process (procedure sTPE 3). Oxygen plasma activation and room temperature were applied as well. Compared with direct printing, more ink would be transferred to the same size area, leading to thicker electrodes which presumably would be more robust to deformation.

Obviously, the geometrical dimensions of the design would be distorted slightly, but it could be dealt with at the design stage. To perform the stretch, a tensile force was applied in a direction parallel to electrodes using a clip system (Figure 22). The stretching ratio (change in length) was measured.

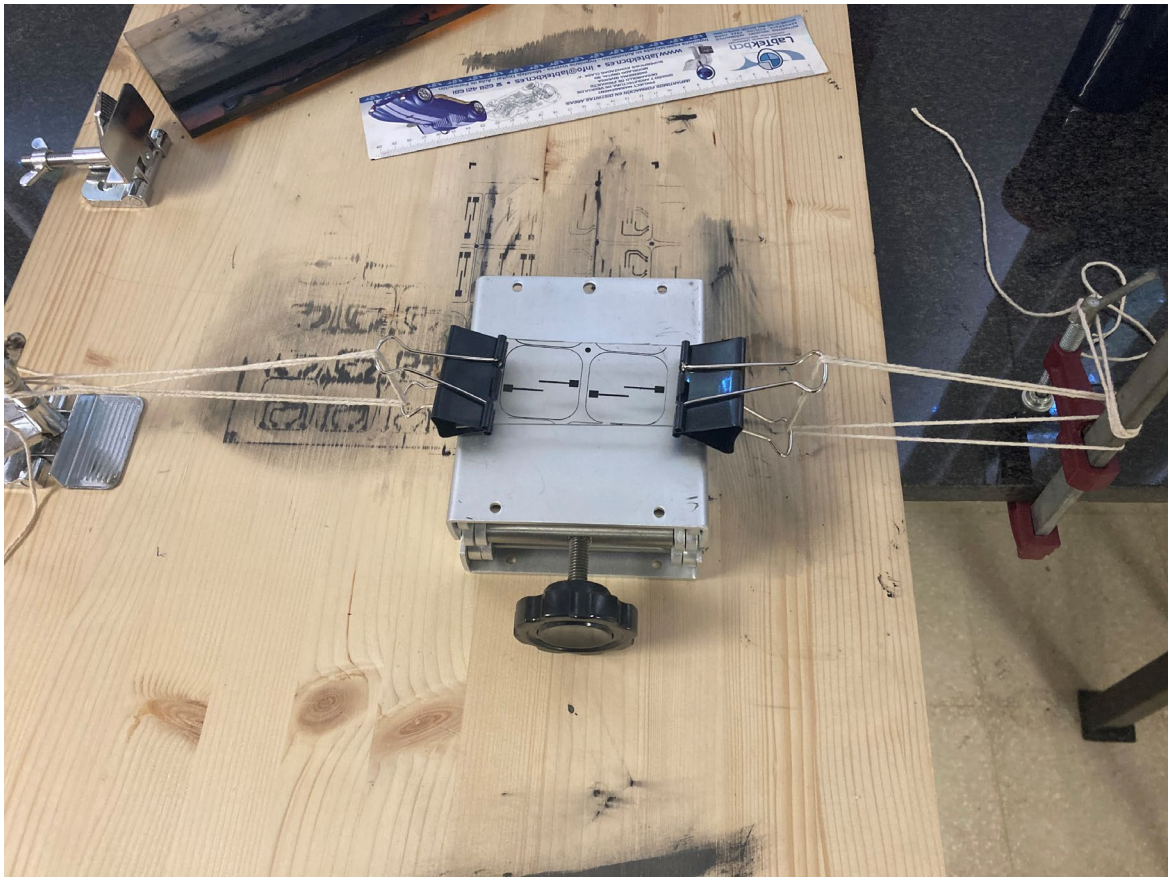

Figure 22. Experimental setup for elongated printing.

Once electrodes were printed, their electrical performance was tested using a multimeter, where their resistance was measured. To test their robustness to deformation, electrodes were bended for ten times and their resistance was monitored again. Thickness of the electrodes was measured using the profilometer.

3.5. Electrochemical characterization

The printed electrodes were designed to function as a conductivity sensor. This means that the measured impedance across electrodes will depend on resistivity of the solution in contact (number of free ions present). The electrochemical performance of the electrodes can therefore be measured using standard conductivity solutions. Draw a line graph of solution concentration and conductivity based on the measurement results. If the linear correlation is met in the range of measurement, this indicates that the performance of the electrode is good.

NaCl solutions of different concentrations (10, 30, 50, 70, 100 mM) were prepared to validate the performance of the designed sensor. The standard conductivity of a solution is measured using a conductivity cell (Jenway Conductimeter). Its corresponding specific conductivity is 1.062, 3.89, 5.1, 7.15 and 10 mS/cm, as shown in Figure 23. Knowing the standard conductivity is key to stablish the constant cell of our sensors.

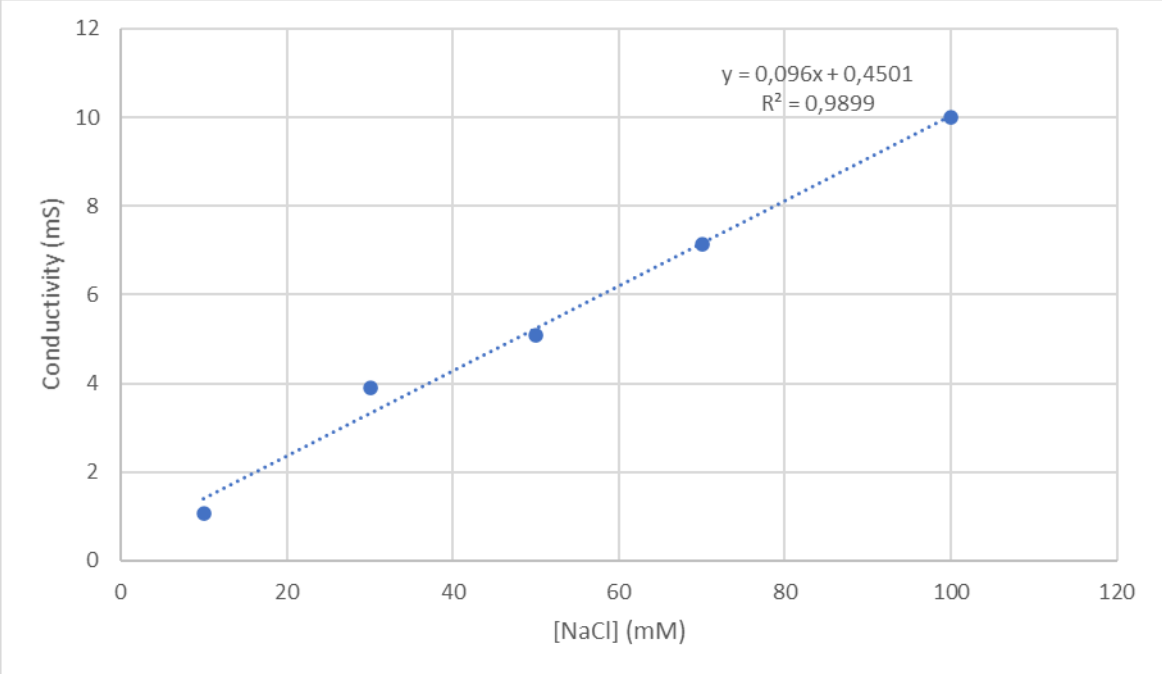

Figure 23 Linear relationship between NaCl solution concentration and specific conductivity.

Measurements with our printed sensors were performed using electrochemical techniques in PalmSens4 portable potentiostat . We performed an impedance spectroscopy applying a potential of 0.25 V AC with scanning frequency from 10 Hz to 10^6 Hz, plus an offset of 1.5 V DC.The measurement procedure consisted in placing a 100 µL droplet of the testing solution on a PDMS frame between the electrodes. This frame ensured that the solution was in contact with the electrodes in the same position each time, as shown in Figure 24.

In order to avoid cross-contamination between samples, the remaining solution on the electrode after each measurement was washed using distilled water.

Once the measurement was completed, the electrodes were taken off and bended 10 times and then reconnected. The above measurement steps were then repeated. The electrode performance when printed on a PET substrate was compared to the new electrodes printed on a sTPE substrate.

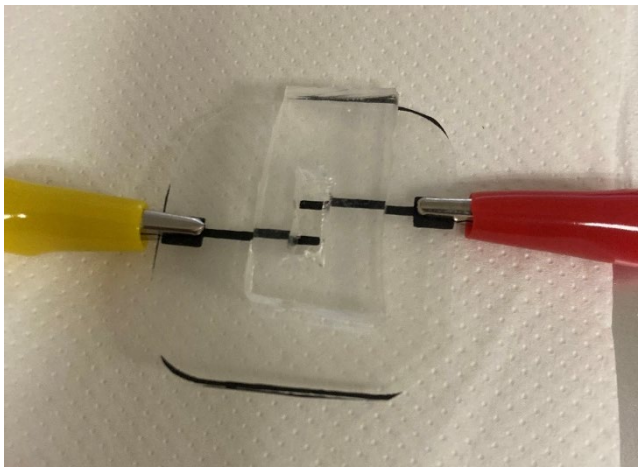

Figure 24 Electrodes for testing and PDMS molds for simulating channels.

4. Results

4.1. Mold fabrication with maskless

Maskless writer for photoresist molds

The photoresist compatible with the maskless writer must be characterized in terms of film thickness and exposure times. Figure 25 shows the relationship between spin speed in the spinner process and thickness achieved for AZ125nxt-10A resist. The results obtained agree with the parameters provided by the supplier and the range of thicknesses obtained, which will eventually result in the height of the microfluidic channels, from 40 um to 120 um is the usual thicknesses used in the old photoresist.

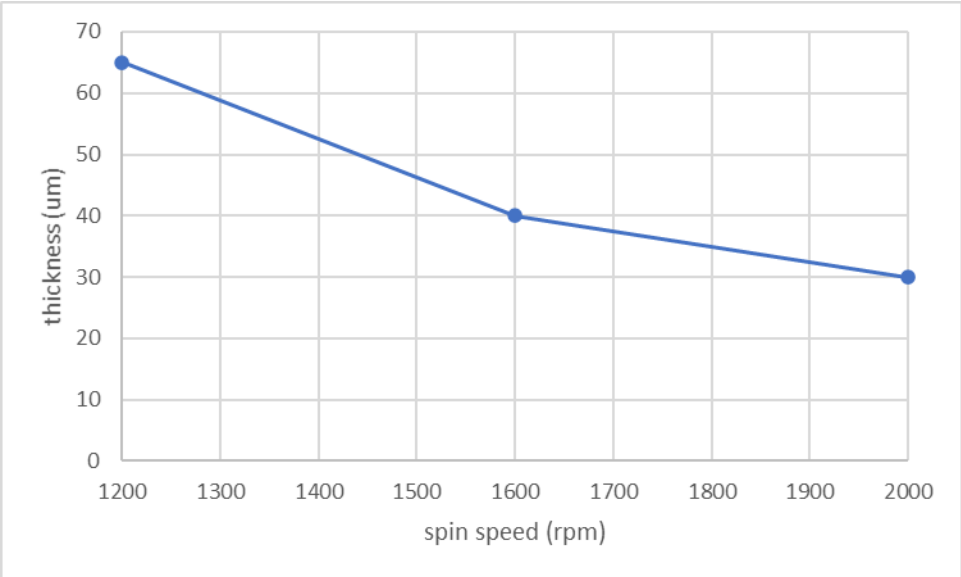

Figure 25 AZ125nxt-10A resist thickness vs spinning speed

It is necessary to fully expose the photoresist to reduce the possibility of exposure deformation. Therefore, it is necessary to obtain optimal exposure conditions. According to the experimental results, it takes about 360 seconds to obtain a photoresist thickness at 1200 rpm.

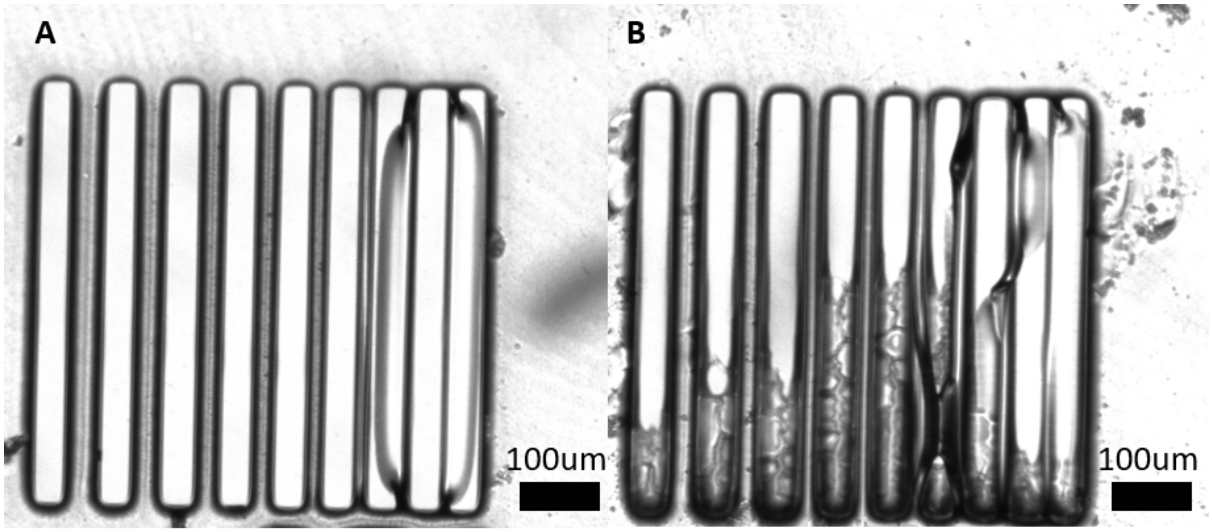

Figure 26 Photoresist molds after exposure for different durations, A) 360s; B) 320s. When the exposure time is insufficient, the mold surface is rougher and the pattern is deformed.

After the printer was calibrated, the resulting exposure results essentially eliminates the gaps between the subimages. For the photoresist mold exposed without using high resolution, the black shadow caused by the uneven height of the channel boundary is more obvious. But no matter whether it is a photoresist mold produced at high resolution or low resolution, the PDMS counter-mold produced by it has completed the microfluidic test. The liquid can pass through the channel smoothly.

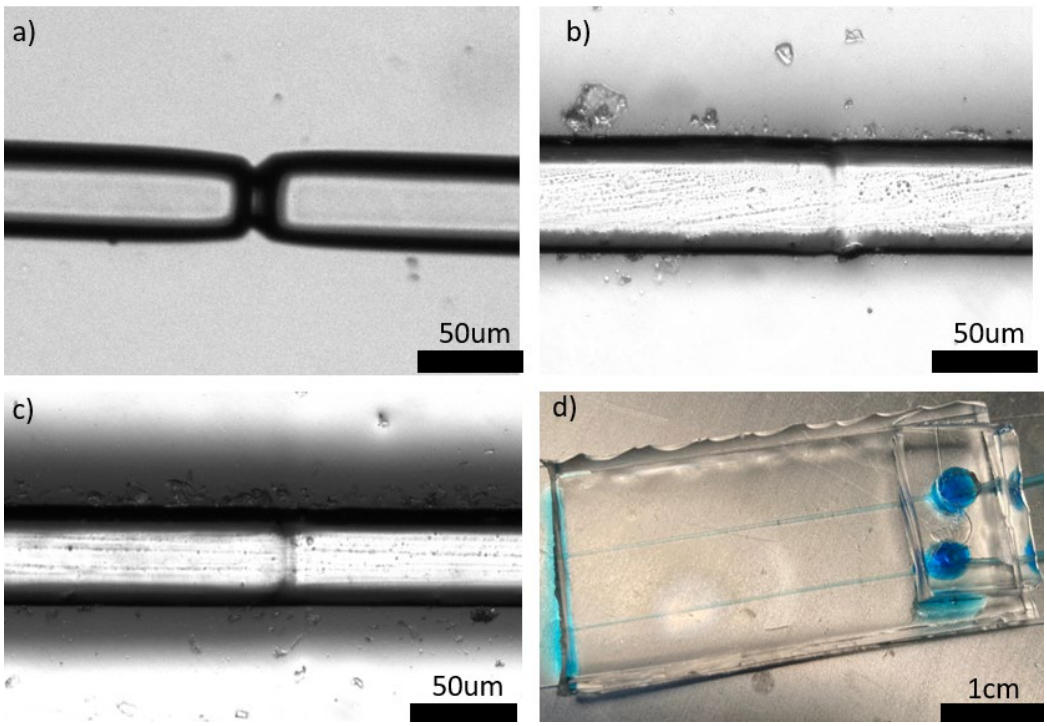

Figure 27 a) For the corrected exposure results, there are obvious gaps between the sub-images. b) Corrected exposure results at high resolution, and using field connection to stitch the images, the gap disappears, and the shadow part of the channel edge is narrower. c) Corrected exposure result at low resolution, the seam is also eliminated, but the shadow

area at the edge of the channel is larger. d) PDMS counter-molds generated using photoresist molds fabricated under conditions b) and c).

By comparing the thickness of the photoresist mold and the relative error of the channel width under the two exposure techniques. The relative error of the maskless technique has the same accuracy as the traditional mask method. The error is less than 7%.

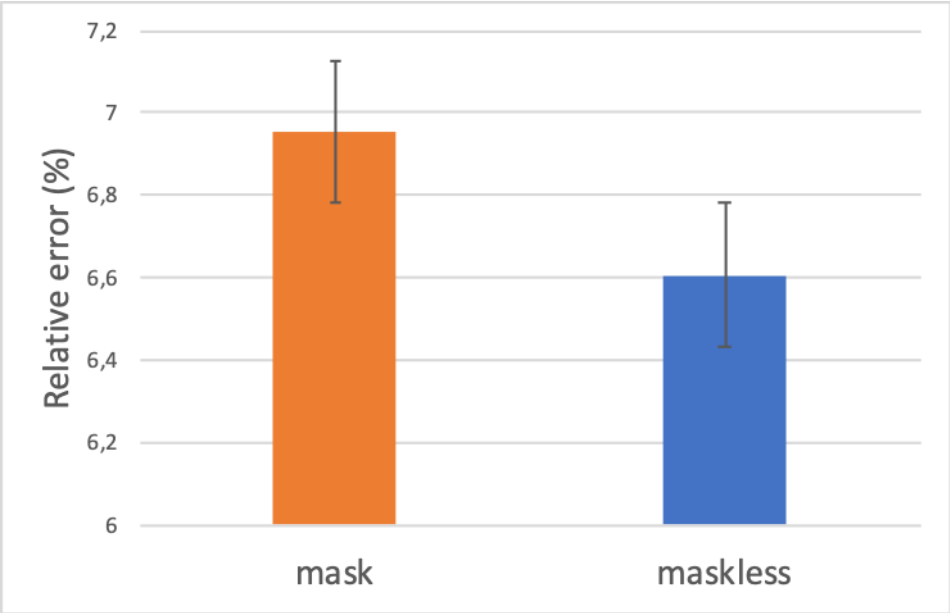

Figure 28 Error comparison between mask exposure and maskless exposure

4.2. Transfer to epoxy mold

Epoxy molds fabricated using an aluminum foil frame and a PDMS frame were compared. With aluminum foil as the outer frame, the epoxy mixture will flow into the bottom of the PDMS mold, resulting in uneven thickness of the epoxy mold and sticking to the aluminum foil. Fragmentation is prone to occur during the final hot pressing process.

First, plasma bonding was used but it modified the chemical interaction between PDMS and epoxy resin, making the unmolding process not possible without breaking the material (Figure 29A).

PDMS turned out as a good option. It does not stick to epoxy so it facilitates the unmolding process and it is readily available in our lab. A frame structure (slab of PDMS of 5 mm height) can be attached to the PDMS mold to be replicated, using conventional bonding strategies between PDMS (Figure 29B).

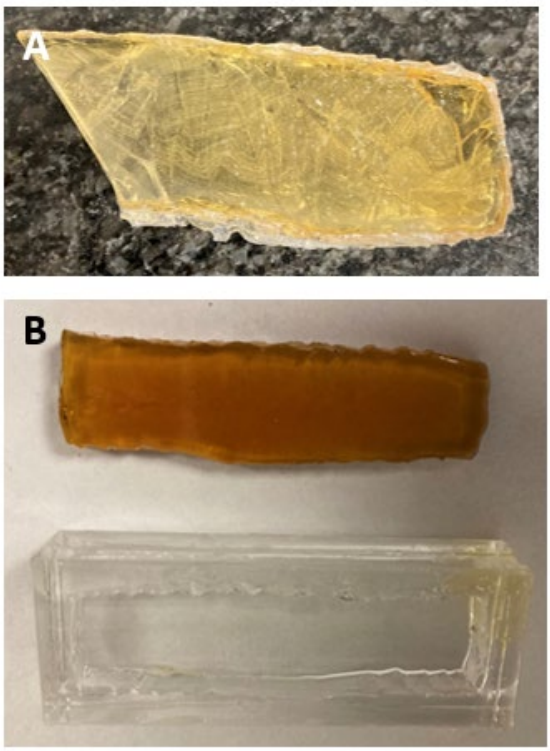

Figure 29 A) Broken epoxy mold after peeling-off of plasma-bonded PDMS frame. B) Well-separated epoxy mold and PDMS frame mold

4.3. Device replication

Hot embossing of sTPE

Table summarizes the optimal conditions to transfer the pattern from the Epoxy mold on the sTPE layer. A higher pressure can make the pattern clearer, but it can easily damage the Flexdym. The duration of heating and cooling is related to whether the structure of the channel is regular.

Table 4 Condition of hot embossing[34].

Temperature	Pressure	HT	CT
120° C	0.5MPa	2min	15min

Comparison between fabrication stages

The relative error width and height deviation between the mold and the part is in all the cases controlled within 7%, shown in figure 30. Therefore, we can conclude that EPOXY moulds produced can be successfully used to transfer the pattern to sTPE layers.

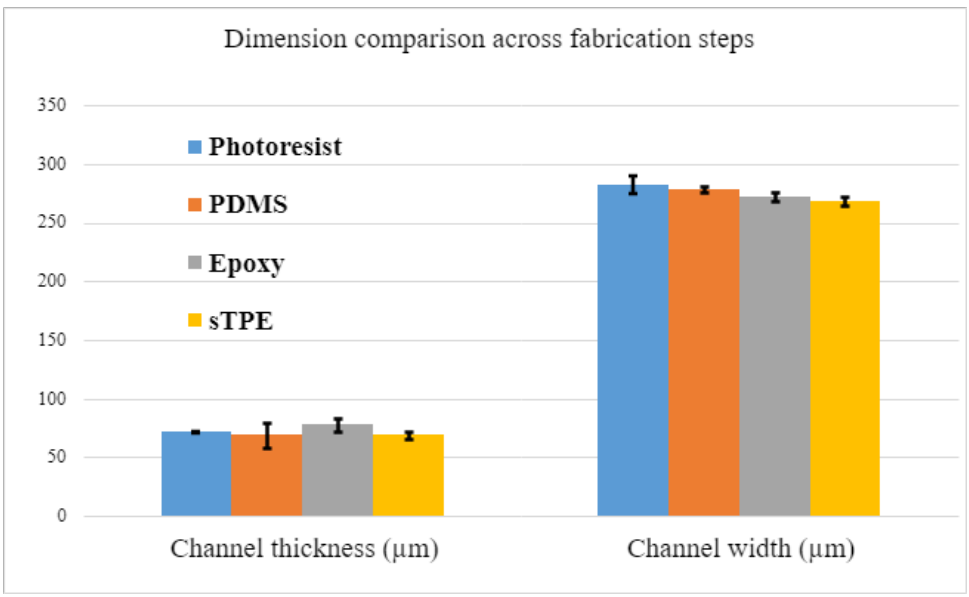

Figure 30 Comparison of the height and width results of molds made of the four materials.

According to the designed protocol, there is no mold breakage. After three replicates, the dimensions of the Epoxy and PDMS molds did not show significant errors. This number of replicates is only significant at lab scale further studies and more resources are needed to completely ensure that the process can be extended to industrial scale.

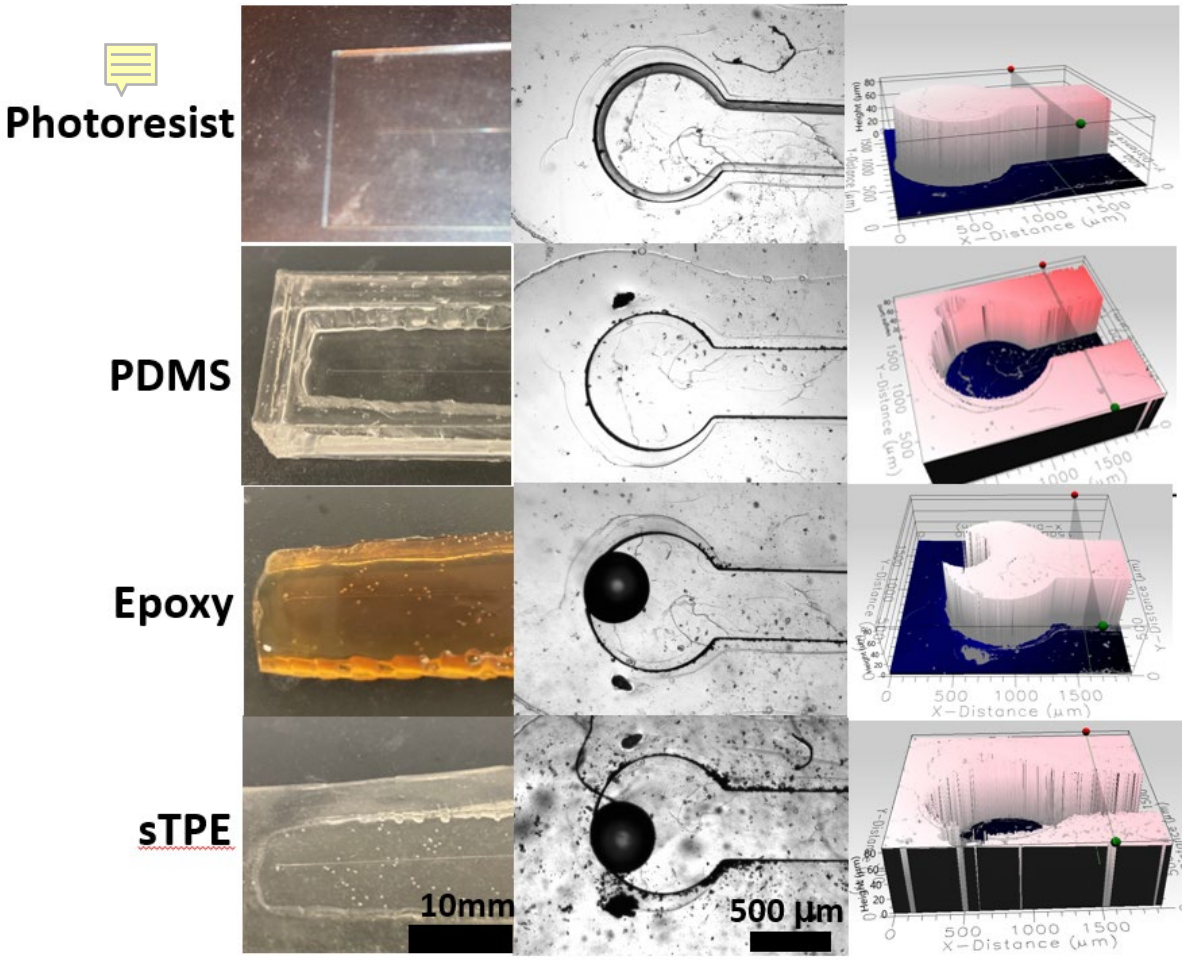

Figure 31 Physical comparison the four materials.

4.4. Electrode printing

A visual inspection of the electrodes after printing shows that on PET electrodes form a continuous, smooth surface, even after the bending deformation (Figure 32). In contrast, electrodes on sTPE did not cover the entire surface with small voids at the borders. These voids produce breaking cracks when the substrate is bended. The same type of structure can be seen in the modified procedure (sTPE 2), oxygen plasma and room temperature curing, with even more clear cracks after the bending. Finally, in the stretched material (sTPE 3) there is not a sign of these voids, with a smooth surface highly similar to the one on PET. After bending, there is a small sign of cracks but they do not seem to break the continuity of the ink, key for electrical performance. The elongation ratio used in sTPE 3 was of the 106.7%.

It is important to notice that although the bending procedure was applied equally, the thickness of the materials used differ slightly (PET: 120 µm and sTPE: 200 µm) which produced forces greater on the sTPE material compared to PET. However, there was a lack of material source in order to try with similar thickness substrates.

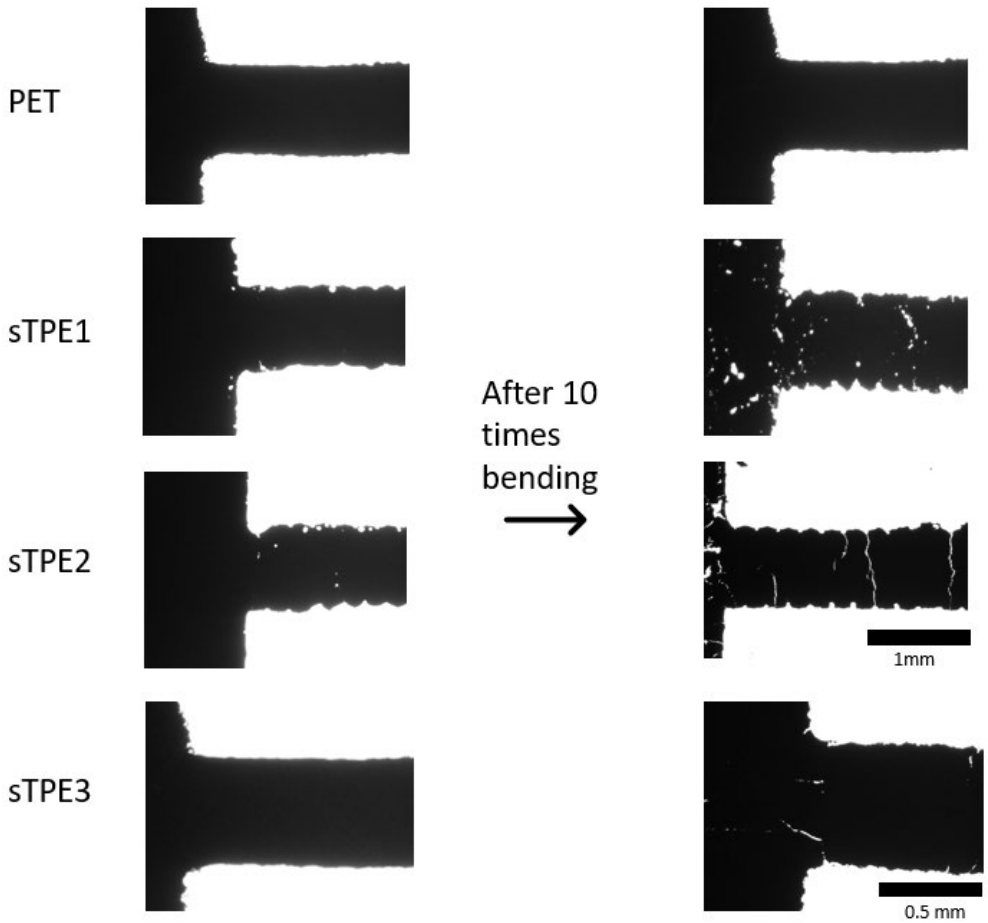

Figure 32. The electrode structure of the two materials under the optical microscope. sTPE2: Oxygen plasma treatment and room temperature drying. sTPE3: Elongation Treatment

Besides the planar dimensions of the electrodes, their thickness is important for their electrical performance because it will define the cross-section available for electron transport. In theory, the quantity of ink provided to the substrate is equal for all procedures as it depends on the silk mask, the ink and the manual applying system, all of them have been kept constant across procedures. Therefore, the thickness of the material can provide information about the ink-substrate interaction as well as the reproducibility of the printing system. As shown in Figure 33, the thickness of electrodes across procedures is quite similar around the 5 microns. The slight decrease in sTPE 1 could be due to the deformation of the sTPE surface due to the high temperature ink curing while the larger increase in sTPE 3 is due to the greater ink quantity provided during the stretching printing.

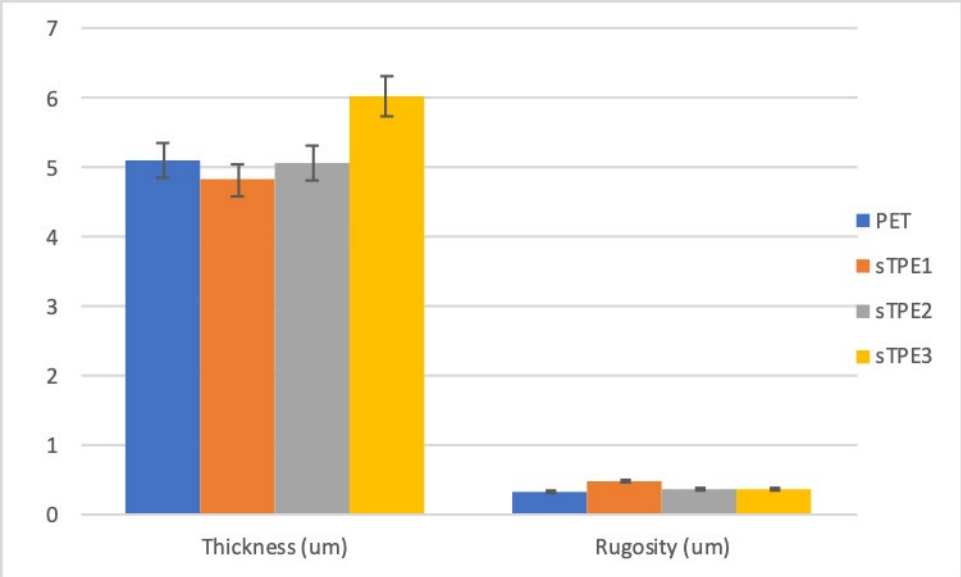

Figure 33 The roughness of the two materials and the thickness of the electrodes printed on them.

.

More important than electrode dimensions, it is their electrical performance. Before testing them as sensors, resistivity of the electrodes can provide a relevant indicator about the status of the electrode and if it is going to work as an electrochemical sensor. In Figure 34, a logarithmic graph summarizes the resistivity measurements of electrodes printed on PET and sTPE before and after bending. Using PET as reference, the original resistivity of the electrodes is close to the 1 kΩ, due to the carbon nature of the electrodes. Carbon electrodes are not specially good conductors, but enough for certain applications such as the conductivity sensor they are intended to be. Moreover, we can see how the bending procedure does not affect the measured resistance, meaning that the integrity of the electrodes has been preserved. For sTPE, it is noted that the resistivity before bending are quite similar to the reference value of PET. They are consistently larger probably due to the imperfections in the surface seen before, which produces a less direct path for electrons. After bending, the cracks that were created break the path, increasing the resistance enormously (more than 100 kΩ) and disabling their use as electrochemical

sensors. On the other hand, with the stretching printing, the measured resistance is closer to the one found in PET (here, the change in dimensions have in effect in that) but, more importantly, the resistance after bending shows just a slight increase, making them still suitable for electrochemical sensing.

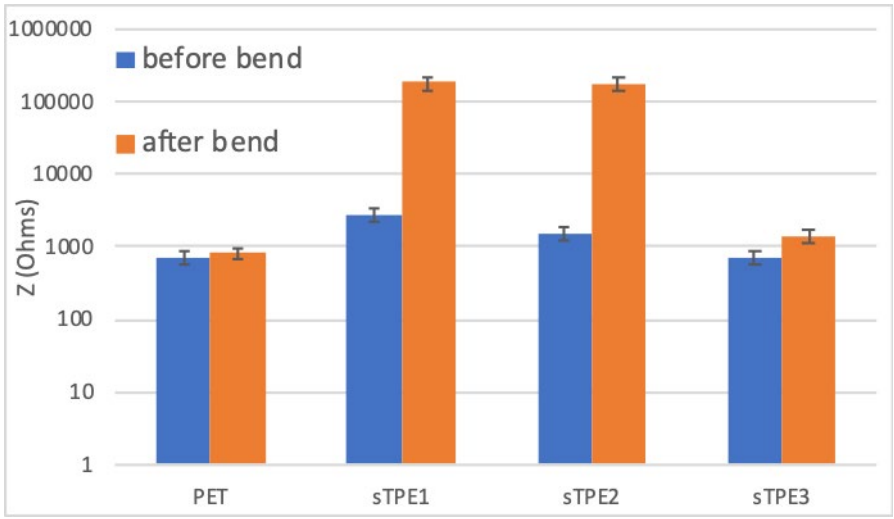

Figure 34 Resistance of different materials. The measurement distance is 1.5 cm. sTPE2: pretreatment with oxygen plasma and dry with room temperature. sTPE3: Elogation treatment

4.5. Conductivity sensor

When sensor performance was tested with different NaCl solutions (of different standard conductivity), the ones printed in sTPE material showed a higher impedance compared to our reference PET sensor (Figure 35). This increase, already seen on the electrode resistance measured in the previous section, depends on the constant cell of the sensor. However, the sensor performance is similar and both of them show a dependence of the sample conductivity. The results showed in Figure 35 for sTPE sensor were obtained from sTPE 2 printing procedure (oxygen plasma pretreatment and room temperature ink curing) because they were more stable.

Besides, in both types of sensors the same behaviour with frequency can be seen. At low frequencies, from 10 to 1000 Hz, the phase of the impedance is capacitive in nature due to the double-layer effect. If frequency is increased, the double-layer capacitance is reduced and the dominant factor is the solution resistance, which is the conductivity of the sample. This can be seen by the flat region at 0º phase between 10^4 and 10^5 Hz region, which would be our chosen frequency for the calibration curve. At even higher frequencies, it is seen again an increase in the phase due to the appearance of the cell capacitance, dominant at high frequencies. This cut offs frequencies depend again on the sensor geometry (constant cell, indirectly), which explains the small differences between both materials.

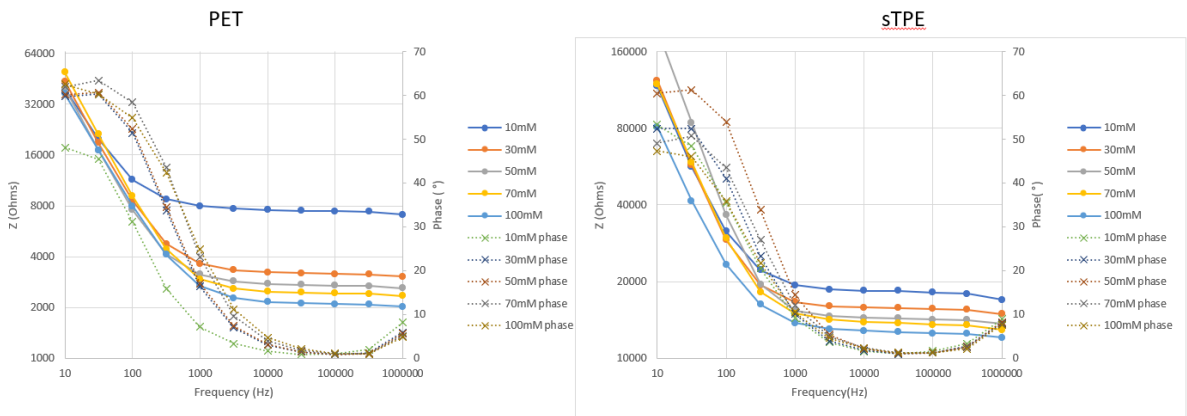

Figure 35 Impedance vs frequency for electrodes of two materials in solutions of different concentrations.

The electrodes of the two materials meet the experimental results. It can be seen from Figure 35 that the conductivity of the PET material is higher than that of the sTPE material at the same concentration. The experimental results of both are also linearly related to the specific conductivity of the solution.

Now, picking the impedance value at 10^4 Hz and converting it into conductivity, they can be compared to the standard conductivities of the solutions used and obtain the constant cell (Figure 36a). The constant cell is the slope of this relation and it is the conversion factor from the conductivities measured by the sensor to the standard ones. Therefore, the constant cell for PET is 24.717 cm^{-1} and for sTPE is 348.19 cm^{-1}. Besides that, a direct relationship with the NaCl concentration can be done, also with a good linearity. This conversion allows to provide total ionic concentration of a solution.

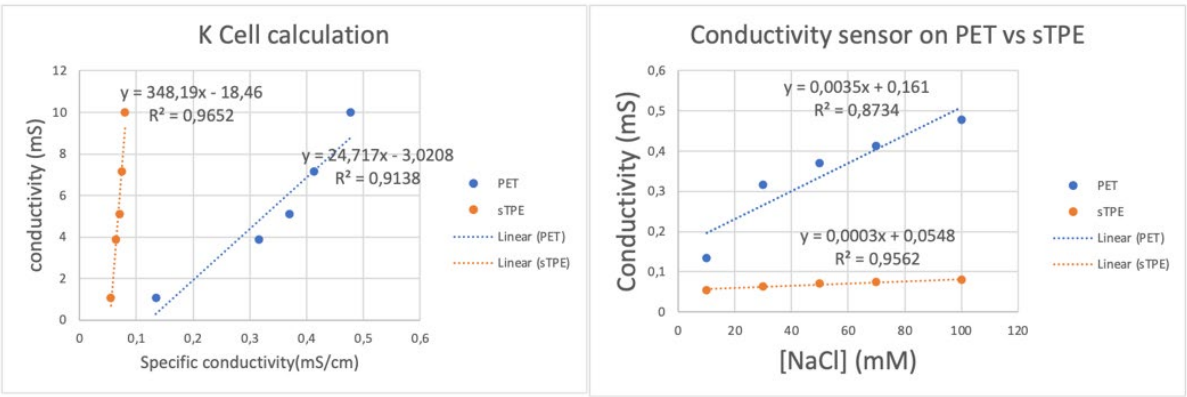

a) b)

Figure 36 a) he relationship between the conductivity with the specific conductivity of the solution. b) The relationship between the conductivity of the electrodes of the two materials at different solution concentrations

Elongation treatment

After validating the use of sTPE as a conductivity sensor, we tried to validate their functionality after being subjected to bending. With PET, there was not a difference in performance after bending, but for sTPE 2 the high increase in electrode resistance (from cracks) makes impossible their use as a sensor.

However, with the sTPE 3, the elongated one, the electrode resistance after bending was not modified greatly and there were no visible cracks. So, the conductivity sensor function after bending may still be active. Therefore, sensor before and after bending were tested (Figure 37b). As it can be seen, the original sensor was working correctly with a slight change in the range of impedance and frequency behavior due to the constant cell modification (dimensions of electrode for elongation). However, when tested after bending, the sensor did not operate correctly and the functionality was lost. The reason behind this loss could be associated to cracks that appear at a smaller scale, which do not have an impact on the overall electrode resistance but in the electrical model of the conductivity sensor.

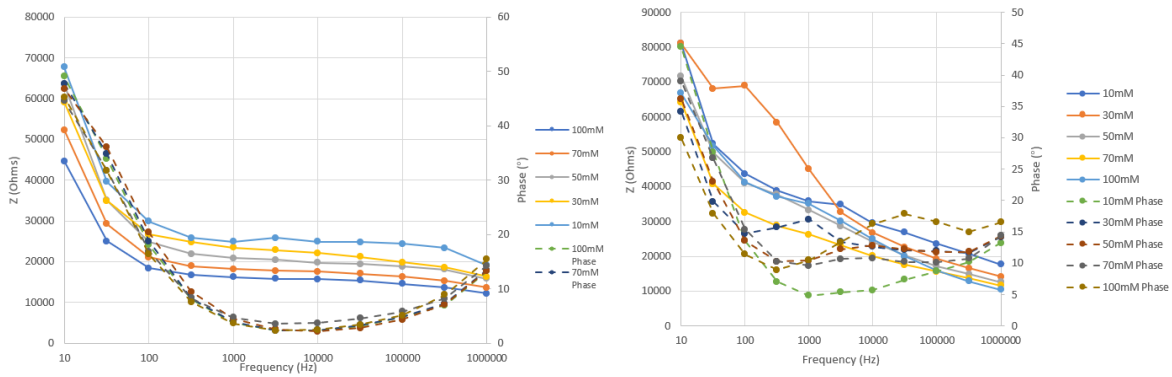

a) b)

Figure 37 Comparison of the relationship between Impedance vs frequency before (a) and after (b) bending of the electrode with elongation treatment.

5. Environment Impact

The project takes into account appropriate environmental factors.

The two materials that generated waste during the project were Epoxy, Flexdym and PDMS. The two nearly do not produce toxic gas and can be recycled. Epoxy produces a severe pungent odor and needs to be stored in designated waste bins.

During the soft lithography stage, various solutions for development need to be stored in designated tanks.

6. Conclusions

The error of the photoresist master board and the design size manufactured by the maskless lithography technology was slightly smaller than that of the mask method. Used the computer to directly import the designed pattern could save the error caused by the mask.

Used resin instead of PDMS to manufacture the mold required for hot embossing, the desired pattern could be obtained on the final sTPE product. And in a certain number of times of service life, used sTPE material as a substrate to print electrodes, the results cannot achieve the performance of traditional PET materials. Also the graphite electrodes on it were very brittle and cannot withstand bending. After use the elongation treatment, its performance had been improved to a certain extent, but it still cannot reach the performance of PET and cannot solve the fragmentation.

6.1. Future development

Change the speed of the spin coater to get more data on the speed and thickness of the AZ125 photoresist. And the does test is repeated to determine the exposure time required for different thicknesses.

Do more hot stamping tests to determine the life of the resin mold. And look for a better transfer process to extend the life of the mold.

According to the elongation process of the electrode, the pattern of the screen mold is designed according to its elongation ratio. Increase the stretching force and measure the performance of the printed electrodes at different elongation ratios.

Bibliography

1. Weibel DB, DiLuzio WR, Whitesides GM. Microfabrication meets microbiology. *Nat Rev Microbiol*. 2007;5(3):209-218. doi:10.1038/nrmicro1616

2. Lachaux J, Alcaine C, Gomez-Escoda B, et al. Thermoplastic elastomer with advanced hydrophilization and bonding performances for rapid (30s) and easy molding of microfluidic devices. *Lab Chip*. 2017;17. doi:10.1039/C7LC00488E

3. Quero JM, Perdigones F, Aracil C. Microfabrication technologies used for creating smart devices for industrial applications. *Smart Sensors MEMS Intell Sens Devices Microsystems Ind Appl Second Ed*. Published online 2018:291-311. doi:10.1016/B978-0-08-102055-5.00011-5

4. Positve-Tone vs Negative-Tone Photoresist - Hanna Naquines. 4 Aug, 2022, from https://openwetware.org/wiki/Positve-Tone_vs_Negative-Tone_Photoresist_Hanna_Naquines

5. Flow P. SU-8 2-25 Permanent Negative Epoxy Photoresist. https://kayakuam.com/wp-content/uploads/2019/10/KAM-SU-8-2-25-Datasheet-9.3.20-final.pdf

6. Scott SM, Ali Z. Fabrication methods for microfluidic devices: An overview. *Micromachines*. 2021;12(3). doi:10.3390/mi12030319

7. Chang CY, Yang SY, Chu MH. Rapid fabrication of ultraviolet-cured polymer microlens arrays by soft roller stamping process. *Microelectron Eng*. 2007;84(2):355-361. doi:10.1016/j.mee.2006.11.004

8. De Graaf RA, Karman AP, Janssen LPBM. Material properties and glass transition temperatures of different thermoplastic starches after extrusion processing. *Starch/Staerke*. 2003;55(2):80-86. doi:10.1002/star.200390020

9. Takeichi T, Furukawa N. *Epoxy Resins and Phenol-Formaldehyde Resins*. Vol 5. Elsevier B.V.; 2012. doi:10.1016/B978-0-444-53349-4.00157-6

10. Eden Tech. 15 Aug, 2022, from https://eden-microfluidics.com/eden-materials/flexdym-pack-alternative-to-pdms/

11. Sales FCP, Ariati RM, Noronha VT, Ribeiro JE. Mechanical characterization of PDMS with different mixing ratios. *Procedia Struct Integr*. 2021;37(C):383-388. doi:10.1016/j.prostr.2022.01.099

12. Johnston ID, McCluskey DK, Tan CKL, Tracey MC. Mechanical characterization of bulk Sylgard 184 for microfluidics and microengineering. *J Micromechanics Microengineering*. 2014;24(3). doi:10.1088/0960-1317/24/3/035017

13. The Epoxy Experts A Division Of Polymer Composites, Inc. 15 Aug, 2022, form https://theepoxyexperts.com/shore-hardness/

14. Cha J, Kim J, Ryu S, Hong SH. Comparison to mechanical properties of epoxy nanocomposites reinforced by functionalized carbon nanotubes and graphene nanoplatelets. *Compos Part B Eng*. 2019;162:283-288. doi:10.1016/j.compositesb.

15. S. J. Hong, S. Choi, Y. Choi, M. Allen, G. S. May, in IEEE/SEMI Advanced Semiconductor Manufacturing Conference and Workshop, IEEE, Piscataway, NJ 2004, pp 404–408.

16. SPS semiconductor production systems https://www.sps-international.com/product/polos-microprinter---up-to-4quot-100mm/22962/

17. Darwin microfluidics. 17 Aug, 2022, from https://darwin-microfluidics.com/products/maskless-soft-lithography-uv-system

18. SPS - User manual for POLOS MicroPrinter

19. M. Worgull, J.-F. Hétu, K. K. Kabanemi, and M. Heckele, "Hot embossing of microstructures: characterization of friction during demolding," Microsyst.Technol., vol. 14, no. 6, pp. 767–773, 2008, doi: 10.1007/s00542-007-0492-0

20. M. Sahli, T. Barrière, and J.-C. Gelin, "Finite element simulation and experimental investigation of hot embossing of thin polymer film," Int. J. Simul. Multidiscip. Des. Optim., vol. 4, no. 2, pp. 101–106, 2010, doi: 10.1051/ijsmdo/2010013.

21. A. Ziyara, F. Çoğun, C. Varol, O. Totuk, and E. Yildirim, "Optimization of Hot Embossing Process for Fabrication of Microfluidic Devices," 8th Eng. Technol. Symp., no. May, pp. 61–64, 2015, [Online]. Available: https://www.researchgate.net/publication/279970861.

22. Bhattacharjee N, Urrios A, Kang S, Folch A. The upcoming 3D-printing revolution in microfluidics. *Lab Chip*. 2016;16(10):1720-1742. doi:10.1039/c6lc00163g

23. Amjoud M, Maury F, Soukane S, Duverneuil P. Making of specific electrodes by CVD. *Surf Coatings Technol*. 1998;100-101:169-172. doi:https://doi.org/10.1016/S0257-8972(97)00609-9

24. Ye Z, Li Q, Zhang R, Zhang P, Gui L. Fabrication of a thin PDMS film with complex liquid metal electrodes embedded and its application as skin sensors. *RSC Adv*. 2022;12(14):8290-8299. doi:10.1039/D1RA09394K

25. Xu X, Luo M, He P, Guo X, Yang J. Screen printed graphene electrodes on textile for wearable electrocardiogram monitoring. *Appl Phys A Mater Sci Process*. 2019;125(10):1-7. doi:10.1007/s00339-019-3006-x

26. Chakraborty S, Das C, Saha R, et al. Investigating the quasi-oscillatory behavior of electrical parameters with the concentration of D-glucose in aqueous solution. *J Electr Bioimpedance*. 2015;6:10. doi:10.5617/jeb.2363

27. Timmer, B., Sparreboom, W., Olthuis, W., Bergveld, P., & van den Berg, A. (2002). Optimization of an electrolyte conductivity detector for measuring low ion concentrations. *Lab on a Chip*, *2*(2), 121–124. https://doi.org/10.1039/b201225a

28. Yuan, Z., Hou, L., Bariya, M., Nyein, H. Y. Y., Tai, L.-C., Ji, W., Li, L., & Javey, A. (2019). A multi-modal sweat sensing patch for cross-verification of sweat rate, total ionic charge, and Na + concentration . *Lab on a Chip*. https://doi.org/10.1039/c9lc00598f

29. Massart DL, Dijkstra A, Kaufman LBT-T and I in AC, eds. Chapter 6 Sensitivity and limit of detection. In: *Evaluation and Optimization of Laboratory Methods and Analytical Procedures*. Vol 1. Elsevier; 1978:143-156. doi:https://doi.org/10.1016/S0167-9244(08)70050-7

30. Ting LH, Rodriguez ML, Sniadecki NJ. Effect of Silanization Film Thickness in Soft Lithography of Nanoscale Features. 2011;2(November):1-5. doi:10.1115/1.4005665

31. Sonelastic, Modulus of elasticity and Poisson's coefficient of polymeric materials https://www.sonelastic.com/en/fundamentals/tables-of-materials-properties/polymers.html

32. Homola T, Wu Y, Černák M. Atmospheric Plasma Surface Activation of Poly(Ethylene Terephthalate) Film for Roll-To-Roll Application of Transparent Conductive Coating. *J Adhes*. 2014;90:296-309. doi:10.1080/00218464.2013.794110

33. Eden Tech, Epoxym Kit: Mold Replication Solution https://eden-microfluidics.com/eden-materials/epoxym-microfluidics-mold-solution .

34. Arnau Serra. Sagués Estudi de la fabricació de canals microfluídics en làmines polimèriques i la seva unió mitjançant hot embossing i processos d'unió térmica. Jan 2021.

Appendices

Appendix A - Master fabrication protocols

A1 Conditions for GM1070, 70 µm

1. Materials: Hotplates 65º and 95º, Alarm Clock, Tweezers, Acetone, Propanol, SU-8.
2. Glass slide cleaning (Wash with DI water, dry, Acetone, Dry, DI water, Dry + Hotplate to evaporate humidity, oxygen plasma.
3. Turn off white lights except the yellow one.
4. Pour SU-8 on glass to avoid creating bubbles while on the spin coater. Acetone to clean spin coater.

   Spin speed: 1200rpm, 53s, 100R/s
5. Hotplate at 65º for 10 min
6. Hotplate 95º for 120 min
7. Stick the mask (ink part in contact with su-8)
8. Put the glass under the UV box and put cleaned glasses on top to press the mask against the mold
9. 8 seconds exposition to UV
10. Hotplate 65º for 10 min
11. Hotplate 95º for 40 min
12. Let it rest for 10 min (Delay time)
13. Immerse the mold in a petri dish with PGMEA developer for 4 min
14. Wash it with propanol

A2 Calibration of pixel size and tilt

Tilt correction

1. Open the settings of the software, in SFTPrint/Settings , o n the top of the software.

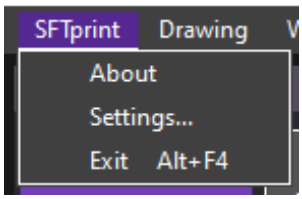

2. Click on the R estart as administrator button

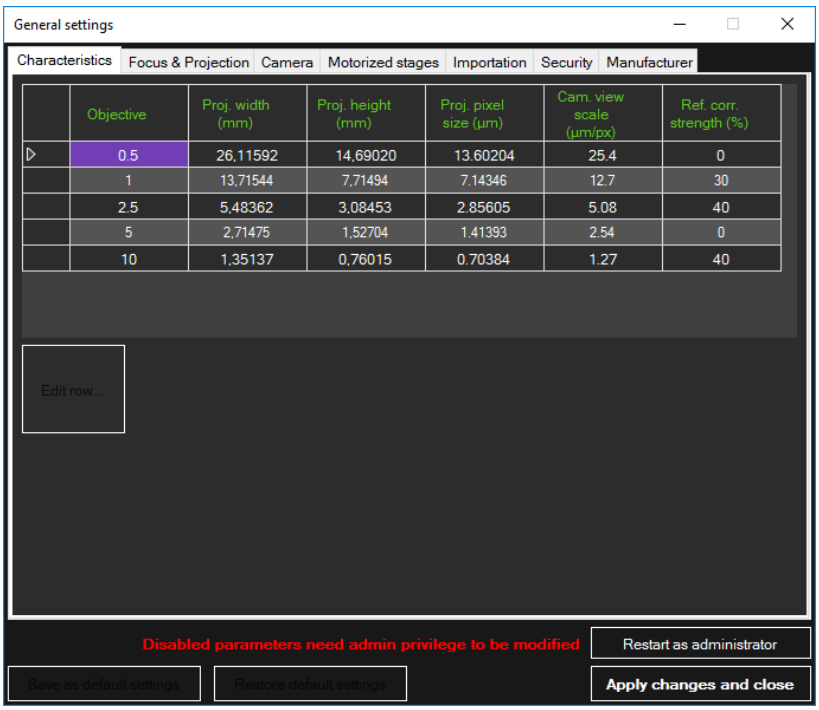

3. Put a piece of silicon wafer with photoresist on top of the holder

4. Choose the appropriate objective on the main screen of the software

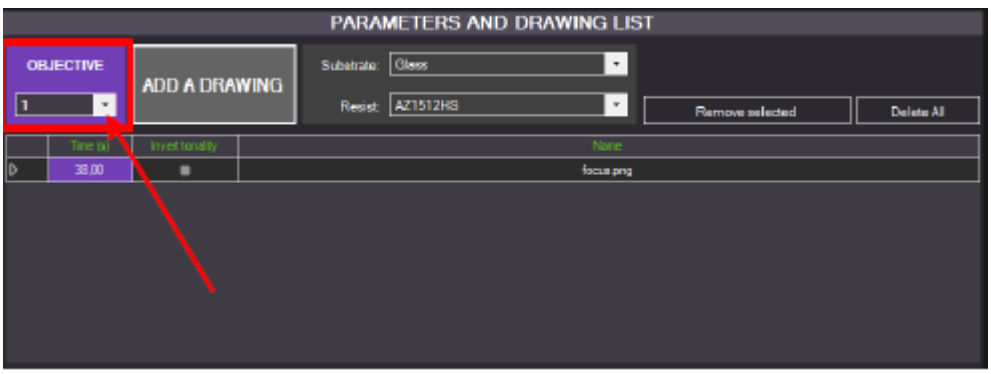

5. Click on the ADD A DRAWING button Select the stitching_HR300 200 image in the folder calibration designs

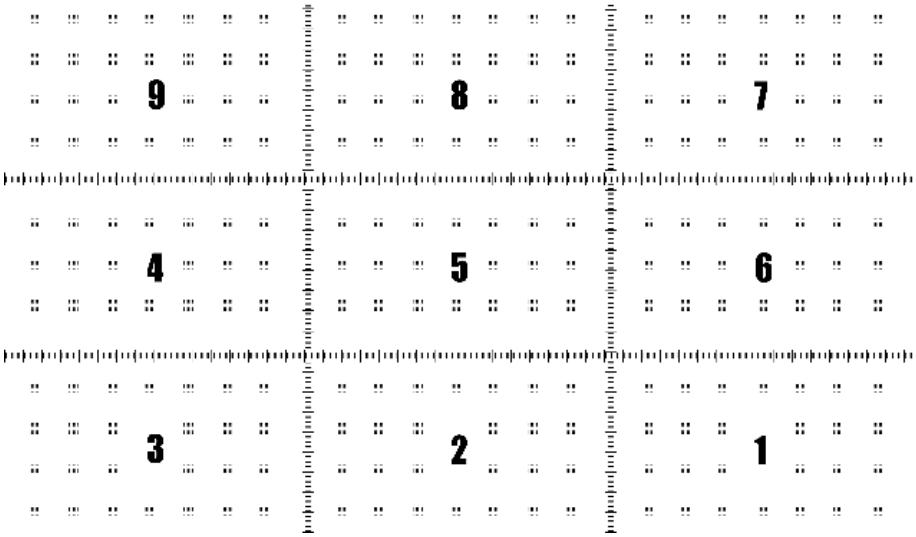

6. A new window, Image size warning , will pop up . S elect the High resolution stitching option and use the following parameters

   x px. red.= 300

   y px. red.= 200

   Then click on STITCH (Black)

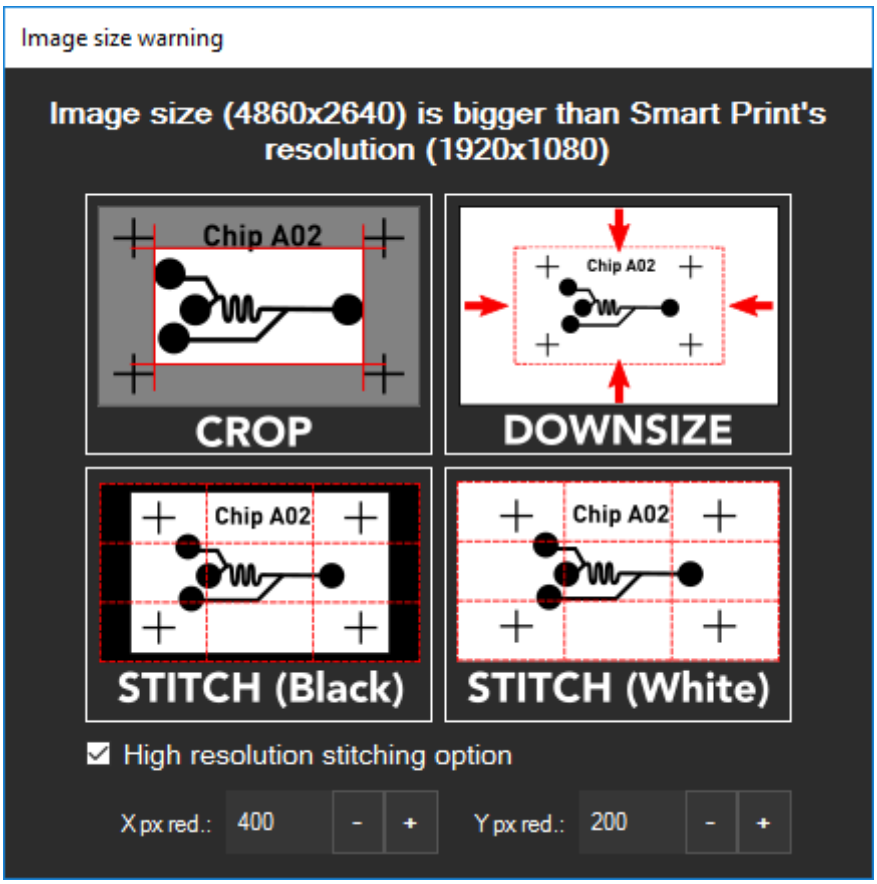

7. Click on the Focus mode button.

8. Click on the Focus mode button to quit this mode. Adjust the focus of the projected image on the camera view (as shown on the picture). Then use the shortcut ctrl + numpad 3 or 9 on the keyboard to move the Z motorized stage. Make the image as sharp as possible. Use the shortcut ctrl + numpad (+ or – to change the speed).

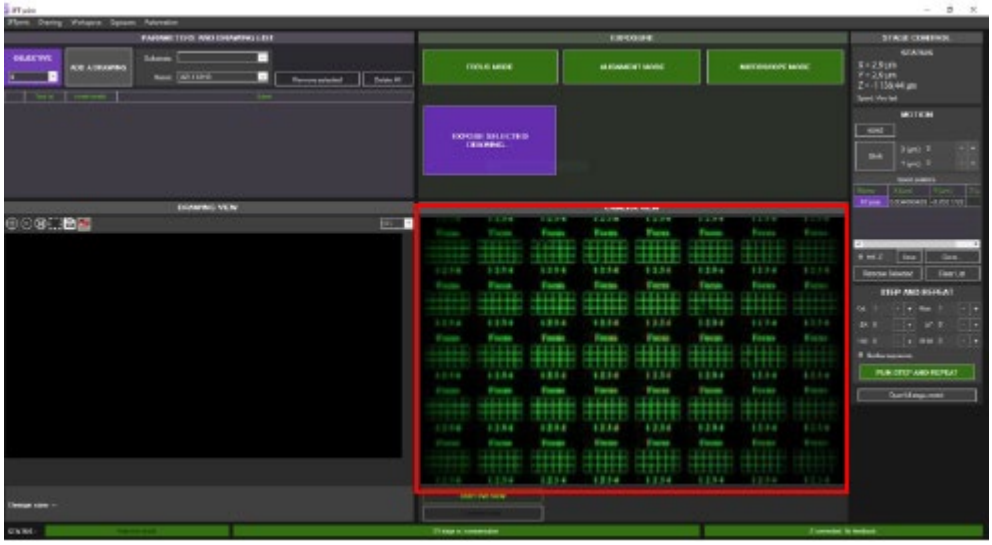

9. On the **parameter panel,** click on **invert tonality**to have in the**image view panel**only the graduation, number and small square inbluecolor.

10. Unload the protection filter, click expose selected drawing

11. Develop the sample and put it back on the sample holder.

12. Click on the microscope mode button on the main screen.

13. Use the XY motorized stage to find the exposed image with the number 5

14. Then move along the X axis to find the graduation between the sub images (as shown on the image). Zoom in the image using the mouse wheel.

15. The calibration consists in match ing the graduation of the two sub images.

16. To do so, calculate the offset (dy) in pixels between the two sub images knowing that the gap between two large graduations is 100 px (as shown on the image) (10 px between two small graduations)

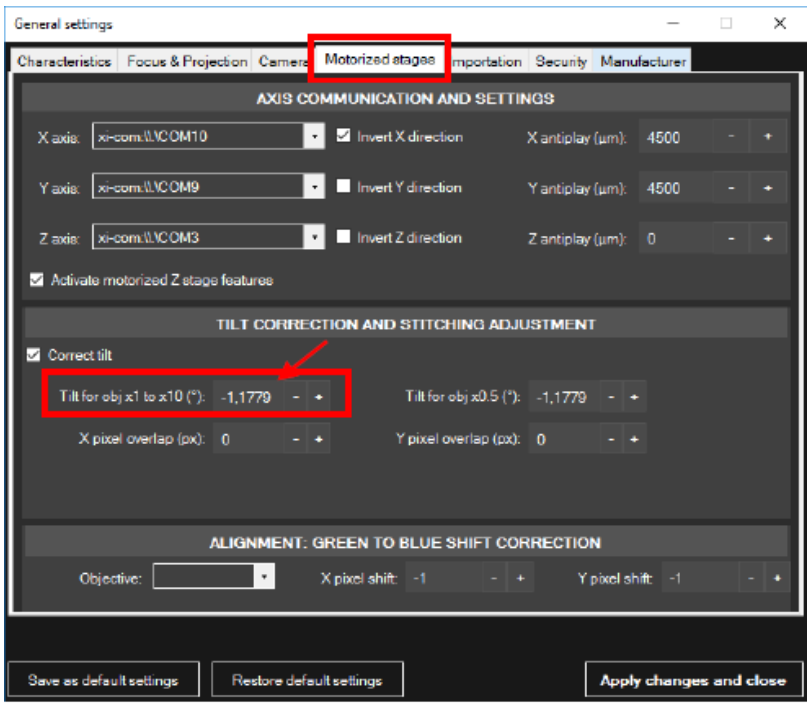

17. Open the settings of the software, in SFTPrint/Settings , on the top of the software. In the Mo torized stage s panel , we will calculate the new value for the tilt correction (θ new)

18. Use the following formula to calculate $\boldsymbol{\Delta\theta}$

    $\Delta\theta = \arctan(dy/1620)$

    Be careful to calculate it in degree (not in radian)

19. Then **calculate the new value for θ**using the following formula: θnew= θ ± Δθ
    Note the valuescalculated with +Δθ and -Δθ

20. **Replace the current value by the θnew value calculated with +Δθ**,then do a new lithography away from the first one.

21. Go to the position of the **sub-image number 5**and check the result of the stitching. If the result is worst(see top image beside) then **replace the valueby the θnew value calculated with -Δθ**and do a third lithography away from the first and second one. If the Δθ has been measured correctly the graduations should match as shown on the image beside (bottom).If the result is not perfect the procedure can be done one more time.

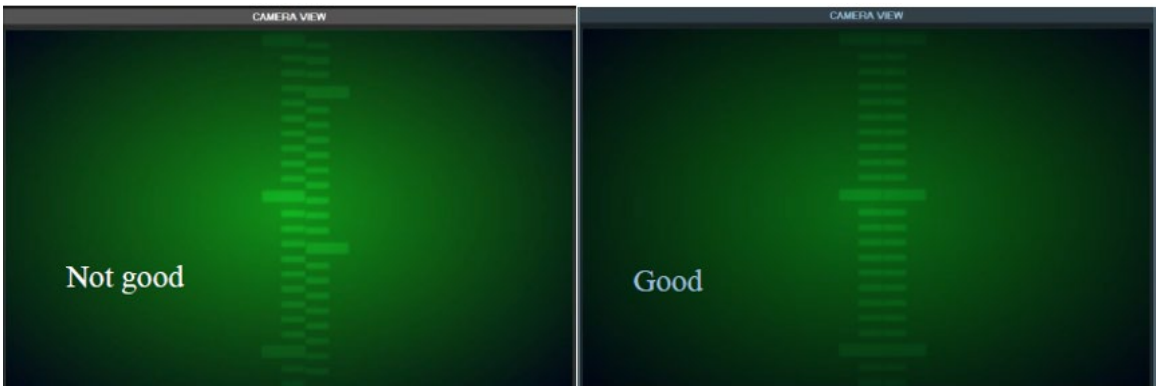

22. Once the correct value has been determined,click on the **Save as default settings**button on the Motorized stages panel of the General settings. Then click on the **Apply changes and close** button.

Pixel size correction:

The size of the projected pixels must be adjusted to make sure that there is no gap between the exposed sub-image composing a stitched file neither an excessive overlapping.

To do so, the same calibration grid used for the tilt correction can be used. Select an objective and expose the calibration grid in the same conditions as explained previously.

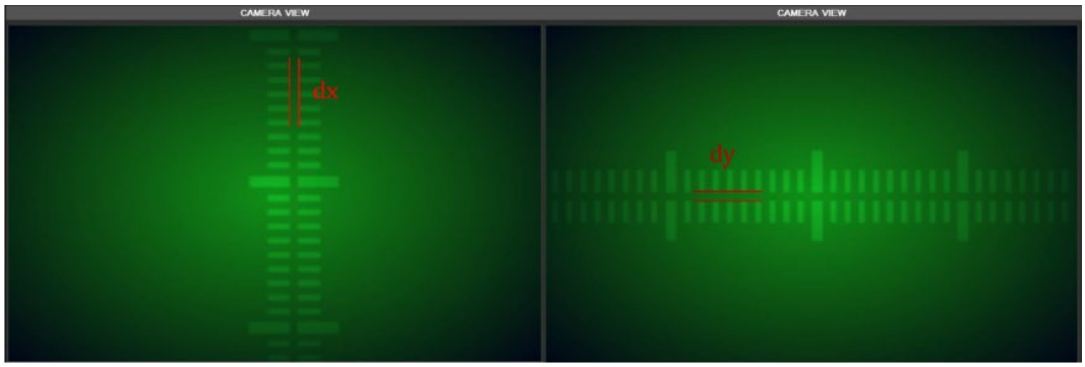

Measure the offset/overlap between two graduations that should be touching to calculate the new pixel size to apply using this equation:

s1 * 1620 = L1
s2 * 1620 = L2 = s1 * 1620 − Δx
L1 + Δx = L2

Hence s2 = (s1 * 1620 – **Δx) / 1620** (or s2 = (s1 * 880 – Δy) / 880 if measuring a shift along the y axis)

s1 : projected pixel size (µm)
s2 : new projected pixel size (µm)
L1 ; L2 : projected field size (µm)
Δx : distance between two graduations along x axis (µm) ***(negative if overlap)***
If necessary, the length of the large scales is 60 px.

The value s1 can be found in SFTprint/Setting/Characteristics.

A3 Conditions for AZ125nxt-10A, 70 µm

1. Materials: Hotplates 120º, Alarm Clock, Tweezers, AZ 300 MIF, AZ125nxt-10A.
2. Glass slide cleaning (Wash with DI water, dry, Acetone, Dry, DI water, Dry + Hotplate to evaporate humidity)
3. Turn off white lights except the yellow one.
4. Pour AZ125nxt-10A on glass to avoid creating bubbles while on the spin coater.

   Spin coating: 300rpm, 5s
   1600rpm, 12s
   400rpm, 15s
5. Hotplate at 120º for 40 min
6. Expose: 360s with g-line

7. Develop: Immerse the mold in a petri dish with AZ 300MIF developer for 50s then clean with DI water, repeat 3 times.

Due to the high resolution, the pattern will be divided into multiple sub-images. There will be gaps and skew between the subgraphs. The writer needs to be corrected.

Tilt correction

Since there is no alignment between subgraphs, the deviation value is dy, and Δθ is calculated by measuring dy, and the θ value is corrected.

Appendix B – PDMS injection mold protocols

1. Treat the finished SU-8 master mold with Chlorotrimethylsilane.
2. Prepare the PDMS solution by mixing the base & hardener according to the manufacturer's instructions (e.g.ratio of 1:10 for Sylgard™184). Evaluate the PDMS volume to get two 3-7mm thick PDMS counter-molds.
3. Desiccate the PDMS mix for at least 30 minutes to remove all air bubbles.
4. Pour an equal volume of PDMS mixture into the prepared glass mold frame.
5. Bake the PDMS for 1-2 hours at 80-90ºC in the oven.
6. Remove the frame from the oven. Unmold PDMS from frame.

Appendix C – Epoxy injection mold protocols

1. Weight the epoxy component A(resin) and B(hardener)) according to the calculation. Then heat up the components separately on a hot plate set at 70ºC for at least 10 minutes.
2. Mix components A and B of the epoxy using a stirrer, Heat at 70ºC.
3. Desiccate epoxy mix for at least 1 hour to get rid of air bubbles.
4. Pour the epoxy liquid slowly into the PDMS mold. Place epoxy in the oven at 120ºC and bake for 20 hours. Note: Make sure the oven shelf is flat.

5. Remove the PDMS mold from the oven. Unmold epoxy from PDMS mold.

6. Bake the epoxy mold at 180ºC for 2hours. To ensure the mold stays flat, we suggest using a heating press for baking or to use a hotplate with a weight on top of the mold.

Appendix D – Flexdym mold protocols

1. Heat the heat press to 120ºC.

2. The Epoxy mold was overlaid on the Flexdym and placed on the heat press.

3. Add the pressure plate down until it touches the epoxy mold. Move the pressure bar up to the high point, then down to a 40-degree angle to the horizontal.

4. Heat press for two minutes with 120ºC.

5. Set the temperature to 0ºC and let the heat plate temperature drop. Hold for 15 minutes.

6. Release the heat platen and remove the mold. Let stand to cool to room temperature.

7. Unmold Flexdym from Epoxy mold.